CHAPTER

4

Coupling Microscale Transport and Tissue Mechanics: Modeling Strategies for Arterial Multiphysics

M. Marino[*], *G. Pontrelli*[†,#], *G. Vairo*[‡], *P. Wriggers*[*]

[*]Institute of Continuum Mechanics, Leibniz Universität, Hannover, Germany [†]Istituto per le Applicazioni del Calcolo (IAC) - CNR, Rome, Italy [‡]Department of Civil Engineering and Computer Science, Università di Roma "Tor Vergata", Rome, Italy

4.1 INTRODUCTION

The complete understanding of the physical mechanisms underlying the correct functioning of the human body, from the cellular to the organ level, stands out as one of the major challenges in modern medicine (Ethier and Simmons, 2007). Indeed, the ultimate goal is to turn heuristic knowledge into predictive capabilities, via the quantitative modeling of the fundamental interactions between basic biochemical processes and biomechanical mechanisms.

In this framework, although cardiovascular diseases are the leading cause of deaths worldwide, their etiology is still often debated and therapeutic approaches are usually driven by risk ranges deduced via clinical records (Fuster and Kelly, 2010). Nevertheless, when addressing, for instance, arterial diseases (such as atherogenesis and aneurysms), it is well-known that pathologies are driven by the biological activity of cells in response to both biomechanical and biochemical stimuli (Taylor and Humphrey, 2009). Unfortunately, the specific causative link between biomechanical/biochemical factors and arterial pathogenesis remains essentially unknown because of the substantial complexity of the biomechanical/biochemical environment affecting arterial tissues.

Many biochemical substances (such as oxygen, nutrients, hormones, enzymes, proteins, tissue inhibitor, regulators of growth, and sometimes drugs) are dispersed in a living body with concentrations controlled by complex regulatory mechanisms (Sagi and Gaffney, 2015; Lilly, 2014; Taylor and Humphrey, 2009). Alterations in transport phenomena play a crucial

[#] Chapter coordinator.

role in tissue inflammatory states, mechanical dysfunctions and damage. As a matter of fact, for instance, the synthesis/degradation of the constituents of the extracellular matrix (ECM) is regulated by cell–cell signaling pathways involving matrix metalloproteinases (MMPs), transforming growth factor-β (TGF-β) and many other molecules (Deguchi et al., 2005; Freedman et al., 2015; García-Alvarez et al., 2006; Jones et al., 2009; Kucich et al., 2002; Rastogi et al., 2013; Sagi and Gaffney, 2015; van der Slot et al., 2005; Visse and Nagase, 2003). In turn, ECM has a major influence on tissue mechanical properties. As a consequence, molecular transport phenomena highly affect the macroscale mechanics of organs and macrobiological structures. Moreover, since biological cells respond to mechanical stimuli by altering the biochemical environment, mechanical quantities have a strong influence on transport phenomena (Ethier and Simmons, 2007; Freedman et al., 2015). Therefore, mechanical and transport mechanisms represent a closed-loop control system characterized by an internal feedback.

Under this perspective, the analysis of physio-pathological mechanisms in organs and macrobiological structures should be addressed via a multiphysics strategy taking into account the two-way interaction between transport processes and mechanics. This would surely open to a better understanding of the onset of many pathologies, as well as to develop novel therapeutic and clinical approaches. For instance, addressing the cardiovascular system, alteration in the concentration of MMPs have been shown to play important roles during the development of cardiovascular diseases (such as plaque formation and rupture, restenosis), highly affecting the mechanical functionalities of cardiovascular structures (Jones et al., 2009; Visse and Nagase, 2003).

This chapter aims to present a multiphysics computational strategy for modeling the previously-introduced coupled mechanical-transport system. This is achieved by accounting for the two-way interaction between mechanical tissue response and transport mechanisms, coupled via biochemically-motivated remodeling laws. The proposed approach opens to the analysis of pathological arterial behavior. It is worth observing that a number of well-established models are available in the specialized literature aiming to describe the evolution of arterial mechanics in disease (Baek et al., 2006; Figueroa et al., 2009; Humphrey and Rajagopal, 2002; Humphrey, 2009; Volokh and Vorp, 2008; Watton et al., 2009), and they are generally referred to as growth and remodeling approaches. Nevertheless, in existing literature, molecular transport mechanisms involved in cell–cell signaling pathways are not accounted for, despite of their well-documented importance. Moreover, the proposed strategy would allow to develop novel computational tools, able to gain effective insights into the physical factors that influence molecular transport processes in otherwise inaccessible locations. As a matter of fact, modeling and computational approaches in conjunction with appropriately designed experiments are helping researchers to better understand the link between biochemical environment and arterial diseases. This also aids in the design of novel devices and the development of novel therapies. For instance, numerical and analytical models have been developed to study the transport of drugs (D'Errico et al., 2015; Pontrelli and De Monte, 2007), of lipoproteins (Dabagh et al., 2009), or of chemoattractants (Leemasawatdigul and Gappa-Fahlenkamp, 2012) through vascular walls. Nevertheless, there are many important transport problems that have not been solved yet or require further attention, especially referring to those coupled with chemical reactions or integrated with tissue mechanics.

The mechanics of arterial tissues is highly nonlinear and anisotropic (Holzapfel et al., 2000; Humphrey, 2002; Taylor and Humphrey, 2009), due to the presence of crimped collagen fibers, whose mechanical response at the microscale is strongly affected by nonlinear molecular and inter-molecular mechanisms at the nanoscale (Fratzl, 2008). A number of constitutive formulations for arterial tissues have been proposed in the literature and remarkable overviews are provided by Holzapfel et al. (2000) and by Humphrey (2002). In the framework of structural approaches, aiming to link model parameters with structural properties of the tissue, the most widely known constitutive model is probably the one by Holzapfel et al. (2000), based on an orthotropic hyperelastic material description and characterized by a clear distinction among arterial principal constituents. Nevertheless, in that model, several collagen nonlinearities (e.g., nanomechanics, cross-link effects, crimped microstructure) are taken into account by choosing an exponential-like representation for the fiber strain-energy density (as in a phenomenological approach), disregarding any direct relationship with micro- and nanoscale mechanisms, and thus losing predictive capability of the model on these issues.

Alternatively, constitutive hyperelastic models of collagenous tissues based on multiscale homogenization techniques have been recently introduced (Maceri et al., 2013; Marino and Vairo, 2013, 2014). These models explicitly incorporate nano- and microscale mechanisms, giving a special insight on the deep link between histology, biochemistry and mechanical response of collagenous tissues. Such an approach allows us to straightforwardly incorporate histological and biochemical alterations and it has been also generalized for including damage evolution at different scales, induced by both mechanical and non-mechanical sources (Maceri et al., 2012; Marino, 2016).

With the aim of coupling transport processes with mechanical response, multiscale constitutive approaches are the most promising methodology because they allow introducing only model parameters with a clear physical meaning, avoiding any phenomenological description. Accordingly, the multiphysics framework proposed in the present work couples a multiscale constitutive description of arterial tissues with a mechanistic modeling of molecular transport, through the definition of remodeling laws based on biochemical evidence.

After a brief overview of some of the main histological–mechanical–biochemical features of arterial tissues in Section 4.2, the multiphysics model is described in Section 4.3. A case study is addressed in Section 4.4, analyzing the effects of ECM remodeling mediated by the transport of MMPs and TGF-β on the compliance of an axisymmetric aortic segment. In detail, proposed results clearly highlight that the alteration of arterial macroscale mechanical properties straight results from the alteration of the tissue biochemical environment. Finally, some concluding remarks are drawn in Section 4.5.

4.2 BRIEF ON ARTERIAL TISSUES

An overview of main histological and mechanical features is presented in Section 4.2.1. Moreover, main transport processes within arterial tissues are described in Section 4.2.2 and some mechanisms involved in tissue remodeling are introduced in Section 4.2.3.

4.2.1 Histology and Mechanics of Arterial Tissues

Arterial walls are made up of three different tissue layers which are named (from inner to outer) the tunica intima, the tunica media and the tunica adventitia (Humphrey, 2002). These three layers are sometimes referred to simply in their shortened version as the intima, the media, and the adventitia. In young and healthy arteries, the intima consists of a single layer of endothelial cells and its thickening is associated with ageing and onset of arteriosclerosis. The media is significantly thicker than the intima and it is made up of concentric layers (named medial lamellar units) consisting of smooth muscle cells embedded in an organized network of loose connective tissue (Clark and Glagov, 1985; O'Connell et al., 2008; Wolinsky and Glagov, 1967). A similar layered structure characterizes the adventitia which in general is thicker than the intima but thinner than the media (Chen et al., 2011).

The three-dimensional histological structure of a single lamellar unit has been recently investigated (O'Connell et al., 2008) and described as a thick sub-layer of elastin sheets, sided by an interlamellar substance made up of water, elastin, smooth muscle cells, and collagen. Collagen results in about 20–30% of the aortic wall dry-weight (Behmoaras et al., 2005) and is organized in crimped fibrils with radius varying from 25 to 50 nm (Merrilees et al., 1987). Fibrils are in turn arranged in both thick and thin bundles (namely, fibers). Electron microscopy scan reveals that the fiber period is on the order of 5 μm and the fiber amplitude-to-period ratio is about 0.2–0.5 (O'Connell et al., 2008).

In both media and adventitia, collagen fibers are arranged in circumferential sub-lamellae. In each of them, collagen fibers are helically wrapped around the vessel axis, so that the collagen fibers are approximately parallel to one another. Fiber orientation of each sub-lamella differs from the adjacent ones resulting in a variation of orientations throughout the mural thickness. Symmetric uni-modal (Chen et al., 2011; O'Connell et al., 2008) and bi-modal (Schriefl et al., 2012) distributions have been reported for the wrapping angle. In general, fiber main orientation is close to the circumferential one in the media and close to the axial one in the adventitia. A schematic representation of arterial histology is depicted in Fig. 4.1.

From a mechanical point of view, the pressure–radius relationship of aortic segments is characterized by a relatively high distensibility at low pressures (associated with the elastin content) and a stiffening response for high pressures (related to collagen) (Wolinsky and Glagov, 1964), see Fig. 4.1. Arterial compliance strongly depends on the highly nonlinear tissue constitutive response which, in turn, is mainly affected by collagen mechanics (Fratzl, 2008). As a matter of fact, in the case of tissues with collagen fibers mainly aligned along a single direction and subjected to an along-the-fiber uniaxial traction test, a progressive fiber straightening and the disappearance of nanoscale kinks within molecules are experienced, resulting in an increase of the overall tissue stiffness. Accordingly, the stress/strain curves are typically J-shaped (see Fig. 4.1) and can be subdivided into three main regions (Buehler and Wong, 2007; Fratzl, 2008; Sasaki and Odajima, 1996):

1. Toe region (strain range, 0–2% circa) is a low stiffness region associated with the removal of the microscopic crimp in collagen fibers.
2. Heel region (strain range, 2–4% circa) is a region associated with a significant stiffening response due to the straightening of labile domains of collagen triple-helices (denoted as molecular kinks) that counteract the entropic forces associated with thermal fluctuations.

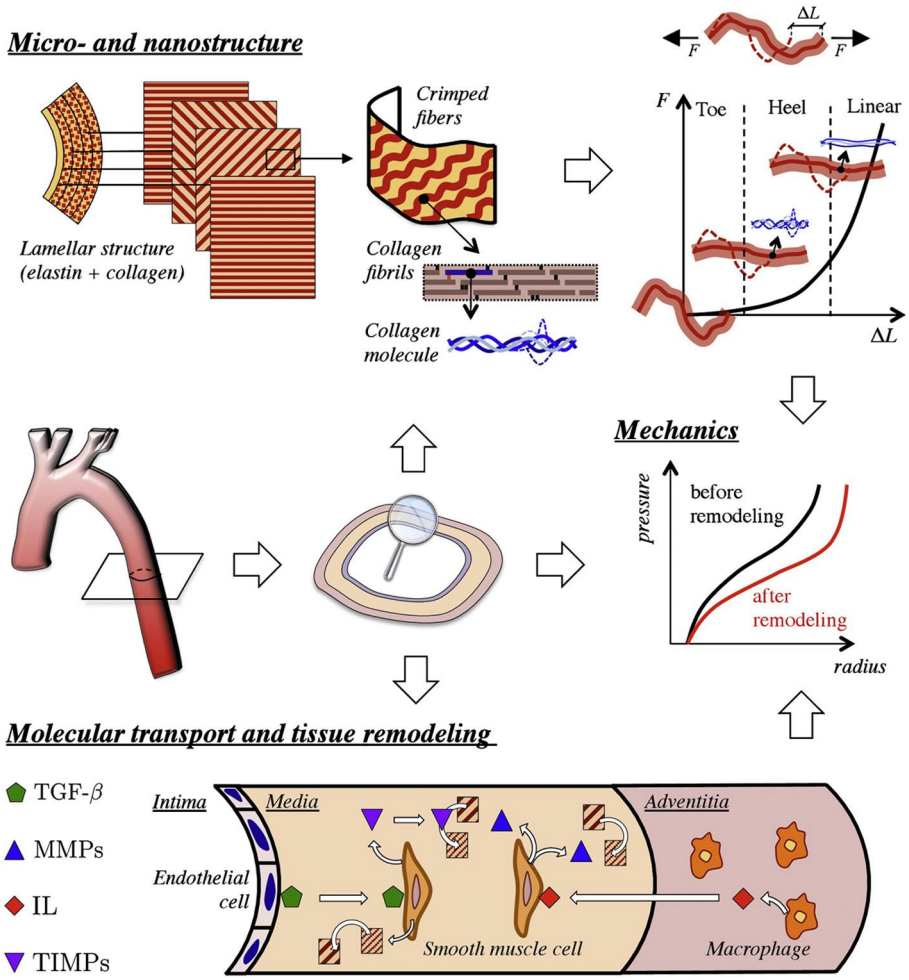

FIGURE 4.1 Multiphysics of arterial response: coupling of arterial micro/nanostructure, mechanics and molecular transport phenomena through the remodeling of tissue constituents: TGF-β, transforming growth factor beta; MMPs, matrix metalloproteinases; IL, Interleukin; TIMPs, tissue inhibitors of MMPs.

3. Linear region (strain range, greater than 4% circa) is a high stiffness region that is mainly related to the stretching of collagen triple-helices and to molecular rearrangement mechanisms (i.e., intermolecular sliding highly affected by covalent cross-links among collagen molecules (Bailey, 2001; Svensson et al., 2013).

Finally, it is worth pointing out that aortic segments in living bodies are pre-stressed and pre-stretched under zero loads: when the vessel is excised, the aortic segment shortens; when a ring cross-section of an artery free of external loads is cut radially, an open sector appears (Kassab, 2006; Rachev et al., 1996; Zhang et al., 2005).

4.2.2 Molecular Transport in Arterial Tissues

Transport mechanisms are involved in physio-pathological paths that are strictly associated with an alteration of arterial mechanical response. As a matter of fact, there is clear evidence that cell–cell communications in the vascular wall can be operated by means of signaling pathways mediated by diffusion of soluble factors, and that the latter contribute to vascular physiological activity, pathogenesis, and disease progression (Lilly, 2014). Some important transport phenomena within arterial tissues are (Lilly, 2014; Taylor and Humphrey, 2009; Sagi and Gaffney, 2015):

- *Oxygen transport.* Biological cells require oxygen and other nutrients for their biological activity which ensure the maintenance of tissue homeostasis. Oxygen diffuses from the luminal surface and, for large blood vessel beyond circa 30 lamellar units, from vasa vasorum in the outer medial and adventitial layers. Severe vascular diseases that thicken the wall (e.g., occlusive atherosclerotic plaques) or increase the distance between the flowing blood and intramural cells (e.g., intraluminal thrombus) affect these transport phenomena and thus the activity of biological cells. As a matter of fact, these diseases are generally related to the development of new blood vessels, or neovascularization, which likely occurs due to chemokines released in response to the local inflammation and/or hypoxic conditions;
- *Transport of vasoactive molecules.* The intimal endothelium produces vasoactive molecules, such as nitric oxide (NO), a potent vasodilator, and endothelin-1 (ET-1), a strong vasoconstrictor. Vasoactive molecules are produced strongly depending on local wall shear stress at the endothelium; they diffuse within aortic thickness and their rate of consumption depends on vascular smooth muscle cells. These molecules play an important role also on arterial growth and remodeling because NO is an inhibitor of smooth muscle cells proliferation and collagen synthesis whereas ET-1 promotes both proliferation and matrix synthesis;
- *Lipid transport.* The development of atherosclerotic process is due to the transport of atherogenic molecules (e.g., low density lipoproteins) between the blood stream and the vessel wall. In this mechanisms, shear-dependent changes in the endothelial permeability have a crucial role;
- *Transport of other molecules.* Cells (e.g., endothelial cells in the intima, smooth muscle cells in the media and macrophages in the adventitia) respond to alterations in mechanical loading via altered gene expression producing, among others, growth factors (such as the transforming growth factor-beta (TGF-β)), cytokines (inflammatory mediators such as interleukines (ILs)), matrix metalloproteinases (MMPs), and tissue inhibitors of MMPs (TIMPs). For instance, the local alteration of intramural stress induces the production and the activation of growth factors (e.g., TGF-β), as well as of MMPs. The latter are also upregulated by indirect effects driven by an altered wall shear stress on endothelial cells and activated by plasmin. In this framework, transport processes are of main importance. As a matter of fact, the media layer (the most important from a biomechanical point of view) is poorly accessible to inflammatory cells but remains accessible to soluble mediators (Michel et al., 2007). A detailed description of signaling pathways involving these molecules is beyond the scope of the present work. As illustrative examples, ILs (produced for instance by macrophages in the adventitia) diffuse up to smooth muscle cells (SMCs) in the media and induce the secretion of MMPs by SMCs. On the other hand, TGF-β (produced for instance by endothelial cells) activates SMCs to express TIMPs which, in turn, inhibit

MMPs. Both TGF-β and MMPs participate in a wide array of cellular responses including: proliferation, angiogenesis, differentiation, apoptosis, inflammation, and wound healing (Jones et al., 2009; Sagi and Gaffney, 2015). Moreover, non-homeostatic concentrations of these molecules affect both composition and organization of constituents of the extracellular matrix. The above-introduced mechanisms (schematically depicted in Fig. 4.1) are further addressed in Section 4.2.3 in terms of remodeling effects.

4.2.3 Extracellular Matrix Remodeling

Extracellular matrix (ECM) is an acellular component of all tissues and organs which provides the necessary physical scaffolding and serves as a source of crucial biochemical and biomechanical signals which, in turn, regulate tissue morphogenesis, differentiation, and homeostasis (Ethier and Simmons, 2007; Sagi and Gaffney, 2015). ECM remodeling is a change in tissue structure, achieved by the reorganization of existing constituents (e.g., altered orientation or cross-linking) or by the synthesis of new constituents. Remodeling may or may not alter the mass density, but it does change tissue stiffness and strength properties which are mainly conferred by the elastin network and collagen fibers, as recalled in Section 4.2.1.

The dysregulation of the degradation and the deposition of the extracellular matrix (ECM) leads to pathological remodeling of cardiovascular tissues which represents an open issue still under investigation (Deguchi et al., 2005; García-Alvarez et al., 2006; Jones et al., 2009; Kucich et al., 2002; Rastogi et al., 2013; Sagi and Gaffney, 2015; van der Slot et al., 2005; Visse and Nagase, 2003). For instance, alterations in collagen cross-linking are often related to connective tissue diseases (such as the Marfan's syndrome) and common cardiovascular pathologies (e.g., restenosis after angioplasty, aortic dilation, dissecting aneurysm, Brüel et al., 1998; Carmo et al., 2002).

Many biochemical pathways intervene *in vivo* when ECM remodels and most of them are open-issues still under investigations. In this framework, a major biochemical mechanisms involves the metabolism of TGF-β, MMPs, ILs and TIMPs. Growth factors TGF-β bind to a specific receptor in SMCs and activates a cascade of events that promote ECM deposition (e.g., deposition of collagen and elastin, Jones et al., 2009; Kucich et al., 2002), affect ECM biochemical features (e.g., inducing collagen cross-linking, van der Slot et al., 2005) and repress ECM degradation (e.g., promoting TIMPs expression, García-Alvarez et al., 2006). On the other hand, MMPs are proteinases that induce ECM degradation (e.g., proteolysis of collagen and elastin, Sagi and Gaffney, 2015; Visse and Nagase, 2003) and affect the disorganization of ECM constituents (e.g., misalignment of collagen fibers, Deguchi et al., 2005; Rastogi et al., 2013). Under normal physiological conditions, MMPs activity is down-regulated, among other mechanisms, by endogenous tissue inhibitors (TIMPs) (Visse and Nagase, 2003; Sagi and Gaffney, 2015). On the contrary, ILs induce the secretion of MMPs by SMC (Lee et al., 1995; Maiellaro and Taylor, 2007).

Under homeostatic conditions, a balance between these mechanisms is maintained in order to tightly control matrix degradation and matrix deposition. A loss of activity control may result in diseases such as arthritis, cancer, atherosclerosis, aneurysms, nephritis, tissue ulcers, and fibrosis (Sagi and Gaffney, 2015; Visse and Nagase, 2003). For instance, within the aneurysmal aorta, this balance is disrupted by an overproduction of MMPs or an underproduction of TIMPs, favoring an enhanced proteolytic state and driving matrix degradation

(Jones et al., 2009; Visse and Nagase, 2003). Thus, while the physiological remodeling process within the arterial wall operates to maintain the physiological arterial function, pathological dysregulation can result in an excessive degradation of critical ECM components, leading to loss of mechanical strength and integrity, and resulting in arterial dilatation, dissection, or rupture (Jones et al., 2009).

Accordingly, the concentration of these molecules within arterial walls are involved in the etiology of many cardiovascular disease, resulting associated with a coupled system made up by arterial biomechanics, transport phenomena and molecular biological activity. The aforedescribed balance between TGF-β, MMPs, ILs and TIMPs (schematically depicted in Fig. 4.1) will represent our study case, addressed in Section 4.4.

4.3 ARTERIAL MULTIPHYSICS MODELING

After a brief introduction of geometrical features and of the general notation (see Section 4.3.1), the general multiphysics rationale is introduced in Section 4.3.2. In the following, possible strategies for modeling each ingredient which builds up the proposed multiphysics approach are described. In detail, arterial mechanics is presented in Section 4.3.3. Thereafter, molecular transport problem is addressed in Section 4.3.4, and biochemically-motivated remodeling laws are defined in Section 4.3.5. Finally, a computational strategy for the coupled problems involved in arterial multiphysics is presented in Section 4.3.6, moving towards an analytical solution.

4.3.1 Geometric Description and General Notation

An arterial segment, $\mathcal{A}$, is regarded as a set of continuously distributed material points $X \in \mathcal{A}$, namely a continuum-body, undergoing a deformation mechanism along the time-path governed by the variable $t \in \mathbb{R}^+$, with $\mathbb{R}^+$ denoting the set of non-negative real numbers (and with $\mathbb{R}^{++} = \mathbb{R}^+ \setminus \{0\}$). Moreover, let $\mathbf{x} = \mathbf{x}(X, t) \in \mathbb{R}^3$ denote the position of a material point X in a three-dimensional Euclidean space at time t, with $\mathbb{R}^n$ denoting an n-dimensional real coordinate space.

For what follows, it is useful to introduce the following terms:

- The mechanical state is described by the current configuration $\Omega = \Omega(t)$ (namely, the region occupied by $\mathcal{A}$ at time t), the second-order right Cauchy–Green deformation tensor $\mathbf{C} = \mathbf{C}(\mathbf{x}, t)$ and the second-order Cauchy stress tensor $\boldsymbol{\sigma} = \boldsymbol{\sigma}(\mathbf{x}, t)$;
- The biochemical environment is defined by the occurrence of M active molecules in Ω and is described by the vector $\mathbf{c} = \mathbf{c}(\mathbf{x}, t) \in \mathbb{R}^M$ where the qth component of $\mathbf{c}$ (namely, $c_q = c_q(\mathbf{x}, t)$) represents the concentration of the qth biologically active molecule in Ω;
- The structural (histological, biochemical, and biophysical) features relevant to tissue constitutive response, s_j, are collected in the set $\mathcal{S} = \{s_1, \ldots, s_S\}$. Due to possible remodeling mechanisms, space-/time-dependency of the values of $s_j \in \mathcal{S}$ is accounted for, namely $s_j = s_j(\mathbf{x}, t)$.

As general notation rules, let $\Sigma = \partial\Omega$ be the boundary of Ω and $\mathbf{n}$ be the outward normal unit vector to Σ. Moreover, let $\mathbf{I}$ be the second-order identity tensor, $\mathrm{Div}(\cdot)$ and $\mathrm{Grad}(\cdot)$ (resp.,

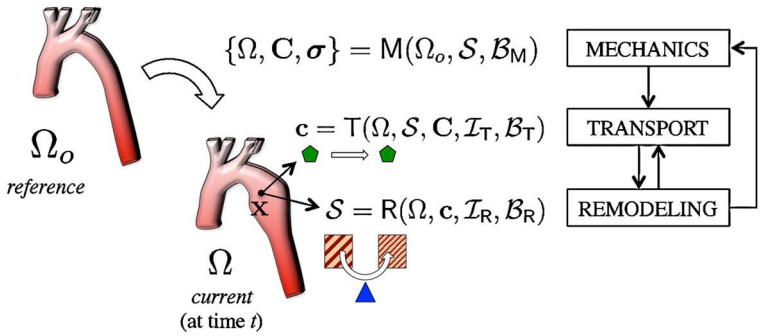

FIGURE 4.2 Multiphysics strategy for arterial behavior: coupling of mechanical M, transport T, and remodeling R problems for obtaining mechanical state $\{\Omega, \mathbf{C}, \boldsymbol{\sigma}\}$, biochemical environment $\mathbf{c}$, and structural features $\mathcal{S}$. Sets $\mathcal{I}_*$ and $\mathcal{B}_*$ respectively collect initial and boundary conditions for problem $* = \{\mathsf{M}, \mathsf{T}, \mathsf{R}\}$.

div$(\cdot)$ and grad$(\cdot)$) be the divergence and gradient operators with respect to the reference (resp., current) configuration. As subscript/superscript notation, the subscript o indicates quantities in the reference configuration, the superscript T denotes the transpose operator, the subscript q implies values in $\{1, \ldots, M\}$, and the subscript j implies values in $\{1, \ldots, S\}$. Finally, $\langle\cdot\rangle$ denotes the Macaulay brackets, that is, $\langle x\rangle = (x + |x|)/2$.

4.3.2 Multiphysics Modeling Rationale

The multiphysics strategy is based on the following ingredients (schematically depicted in Fig. 4.2):

1. *Description of arterial mechanics*. Arterial mechanics is obtained by solving problem M (defined in Section 4.3.3) giving the mechanical state $\{\Omega, \mathbf{C}, \boldsymbol{\sigma}\}$ starting from reference configuration Ω_o, structural parameters $\mathcal{S}$ and the set of mechanical boundary conditions $\mathcal{B}_\mathsf{M}$, namely
$$\{\Omega(t), \mathbf{C}(\mathbf{x}, t), \boldsymbol{\sigma}(\mathbf{x}, t)\} = \mathsf{M}(\Omega_o, \mathcal{S}(\mathbf{x}, t), \mathcal{B}_\mathsf{M})\,. \tag{4.1}$$
Tissue constitutive properties within problem M are defined from a strain-energy density Ψ_T which depends on deformation $\mathbf{C}$ and structural features $\mathcal{S}$, namely $\Psi_T = \Psi_T(\mathbf{C}, \mathcal{S})$;
2. *Description of molecular transport*. The biochemical environment $\mathbf{c}$ is obtained by solving the transport problem T (defined in Section 4.3.4) starting from current configuration Ω, structural features $\mathcal{S}$, strain $\mathbf{C}$ and the set of transport initial $\mathcal{I}_\mathsf{T}$ and boundary $\mathcal{B}_\mathsf{T}$ conditions, namely
$$\mathbf{c}(\mathbf{x}, t) = \mathsf{T}(\Omega(t), \mathcal{S}(\mathbf{x}, t), \mathbf{C}(\mathbf{x}, t), \mathcal{I}_\mathsf{T}, \mathcal{B}_\mathsf{T})\,; \tag{4.2}$$
3. *Description of remodeling laws*. Tissue remodeling is obtained by solving problem R (defined in Section 4.3.5) which gives the values of structural features in $\mathcal{S}$ starting from current configuration Ω, biochemical environment $\mathbf{c}$, and the set of initial $\mathcal{I}_\mathsf{R}$ and boundary $\mathcal{B}_\mathsf{R}$ conditions, namely
$$\mathcal{S}(\mathbf{x}, t) = \mathsf{R}(\Omega(t), \mathbf{c}(\mathbf{x}, t), \mathcal{I}_\mathsf{R}, \mathcal{B}_\mathsf{R})\,. \tag{4.3}$$

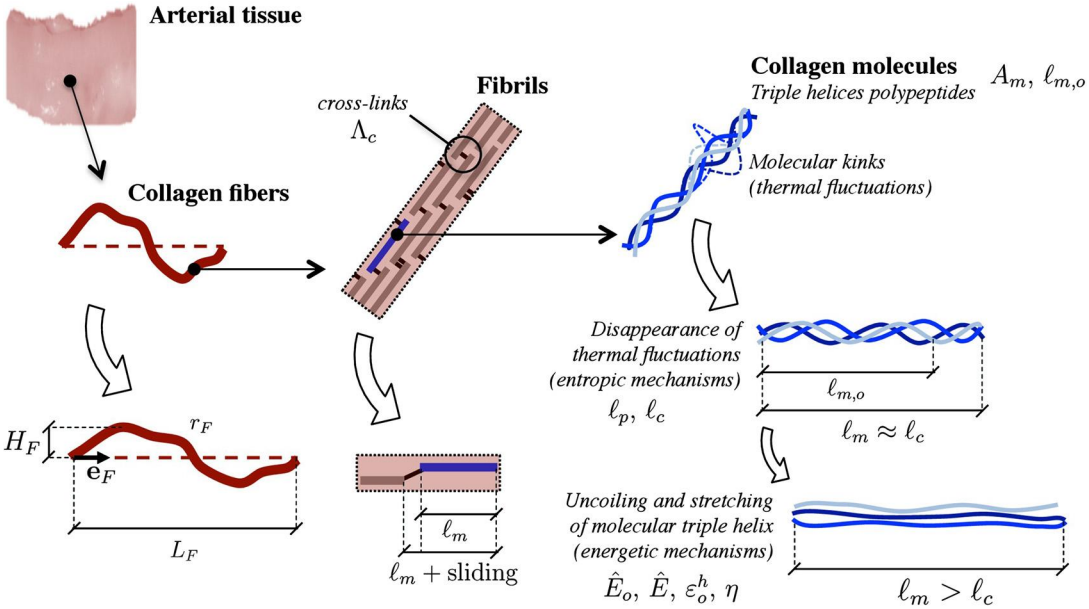

FIGURE 4.3 Collagen-related nonlinearities in arterial tissues – multiscale coupled mechanisms. Symbols are defined in Section 4.3.3.1.

4.3.3 Arterial Mechanical Problem

Arterial mechanics is here described by firstly introducing the nonlinear behavior of collagen fibers in Section 4.3.3.1 which is coupled with a macroscale constitutive description in Section 4.3.3.2, employed in the solving equations for arterial macroscopic response, presented in Section 4.3.3.3.

4.3.3.1 Collagen Multiscale Nonlinearities

Collagen fibers in arterial tissues are characterized by a nonlinear mechanical behavior, related to multiscale coupled mechanisms (see Fig. 4.3). Fibers are assumed to have a circular cross-section of radius r_F (and area measure $A_F = \pi r_F^2$). The crimped structure of collagen fibers is taken into account by considering locally periodic fibers of along-the-chord period length L_F and amplitude H_F in the current configuration (resp., $L_{F,o}$ and $H_{F,o}$ in the reference configuration).

In turn, collagen fibers are bundles of densely-packed fibrils wherein collagen triple-helical molecules (of cross-sectional area A_m and length ℓ_m) are mutually interconnected into a head-to-tail arrangement through intermolecular covalent cross-links, described by their average occurrence per molecule Λ_c. Therefore, fibril mechanics can be described as related to molecular sliding (counteracted by cross-links with stiffness k_c) *in series* with molecular elongation (Maceri et al., 2012; Marino, 2016).

At the nanoscale, the elongation of collagen molecules is governed by in-series entropic and energetic mechanisms (Buehler and Wong, 2007; Fratzl, 2008; Maceri et al., 2012; Marino,

2016). The former are associated with thermal fluctuations (depending on temperature T, molecular persistence ℓ_p and contour ℓ_c lengths, as well as on molecular length $\ell_{m,o}$ in the reference configuration), and the latter with the uncoiling and the stretching of collagen triple helices (depending on low-strain $\hat{E}_o$ and high-strain $\hat{E}$ tangent moduli, molecular uncoiling strain ε_o^h, and uncoiling resistance η).

Accordingly, the set $\mathcal{S}_F$ of histological, biochemical and biophysical features, describing collagen fiber mechanical behavior, results in

$$\mathcal{S}_F = \{\mathcal{S}_f,\ H_{F,o},\ L_{F,o},\ r_F\}\,, \tag{4.4a}$$

$$\mathcal{S}_f = \{\mathcal{S}_m,\ k_c,\ \Lambda_c\}\,, \tag{4.4b}$$

$$\mathcal{S}_m = \{\ell_{m,o},\ \ell_p,\ \ell_c,\ A_m,\ T,\ \hat{E}_o,\ \hat{E},\ \varepsilon_o^h\}\,, \tag{4.4c}$$

where the multiscale nature is highlighted by the inclusions $\mathcal{S}_m \subset \mathcal{S}_f \subset \mathcal{S}_F$.

By following the Maceri–Marino–Vairo multiscale rationale (Maceri et al., 2013; Marino and Vairo, 2013, 2014) (summarized in Appendix A for the sake of completeness), collagen fiber mechanics is defined in terms of their along-the-chord tangent modulus C_F, equal to (Marino and Wriggers, 2016)

$$C_F = E_f \frac{\ell_F^2 + H_F^2}{\sqrt{\ell_o^2 + H_o^2}} \left[\ell_F + \frac{4H_F^2}{3r_F^2\,\ell_F} \left(\ell_F^2 + H_F^2 \right) \right]^{-1}\,, \tag{4.5}$$

where $\ell_F = L_F/4$ and E_f is the tangent modulus of collagen fibrils (see Eqs. (A.1) in Appendix A).

It is worth pointing out that, due to multiscale mechanisms, E_f, ℓ_F, and H_F are functions of the fiber along-the-chord stretch $\lambda_F = L_F/L_{F,o}$. In particular, it results in $\ell_F = \ell_F(\lambda_F) = \lambda_F L_{F,o}/4$, while functions $E_f = E_f(\lambda_F)$ and $H_F = H_F(\lambda_F)$ are determined from inter-scale compatibility relationships, expressed by the system of differential equations (A.6) in Appendix A.

Moreover, it is worth noticing that fibril modulus E_f in Eqs. (A.1) is fully defined in terms of structural parameters $\mathcal{S}_f$. In order to highlight the explicit dependence of fiber mechanical response by the set of structural parameters $\mathcal{S}_F$ in Eqs. (4.4), the functional form $C_F = C_F(\lambda_F, \mathcal{S}_F)$ is conveniently employed in what follows.

4.3.3.2 *Tissue Constitutive Model*

Arterial tissue is regarded as a three-phase substance comprising crimped collagen fibers with volume fraction V_C, a non-collagenous matrix with volume fraction V_M and other non-bearing-load constituents of volume fraction $V_0 = 1 - V_C - V_M$. It is remarked that V_M comprises the volume fraction V_{EL} of the elastin network that bears load (i.e., not including the fragmented elastin), and other constituents of similar stiffness (e.g., cells). Accordingly, V_0 represents the amount of fragmented elastin, degraded collagen as well as other possible non-bearing-load constituents (Maceri et al., 2013; Marino and Vairo, 2013; Rezakhaniha et al., 2011).

Accounting for the lamellar structure of the arterial tissue (see Section 4.2.1), the main direction of collagen fibers in a single sub-lamella is described by the unit vector $\mathbf{e}_F$, in the

following referred to as the fiber-chord direction. Disregarding any curvature effect, collagen fibers are organized in thin planar sheets identified by the orthonormal basis $(\mathbf{e}_F, \mathbf{n}_F, \mathbf{k}_F)$ where $\mathbf{k}_F$ is the normal direction to the tissue plane identified by $(\mathbf{e}_F, \mathbf{n}_F)$. Due to arterial lamellar structure, both volume fractions and collagen orientation are space-dependent functions, even when remodeling mechanisms do not occur (Fig. 4.1).

In the context of nonlinear hyperelasticity, the passive mechanical behavior of the arterial tissue is described by introducing the tissue strain-energy function Ψ_T per unit reference volume from which the Cauchy stress tensor $\boldsymbol{\sigma}$ is obtained as:

$$J\boldsymbol{\sigma} = -p\mathbf{I} + 2\mathbf{F}\frac{\partial \Psi_T}{\partial \mathbf{C}}\mathbf{F}^T\,, \tag{4.6}$$

where $J = \sqrt{I_3}$ with $I_3 = \det(\mathbf{C})$, $\mathbf{F}$ is the deformation gradient, $\mathbf{C} = \mathbf{F}^T\mathbf{F}$ and p acts as a Lagrange multiplier introduced to enforce the incompressibility constraint (namely, $J = 1$) (Auricchio et al., 2013).

In agreement with a constrained mixture approach (Humphrey and Rajagopal, 2002; Humphrey, 2009), tissue strain-energy density Ψ_T is split in collagen-related Ψ_C and non-collagen-related Ψ_M contributions (Holzapfel et al., 2000; Wriggers, 2008). Accordingly, it results in

$$\Psi_T(\mathbf{C}, \mathcal{S}) = V_C\Psi_C(\mathbf{C}, \mathcal{S}) + V_M\Psi_M(\hat{\mathbf{C}})\,, \tag{4.7a}$$

where $\hat{\mathbf{C}} = I_3^{-1/3}\mathbf{C}$ is the isochoric part of deformation. Collagen-related strain-energy contribution is defined as

$$\Psi_C(\mathbf{C}, \mathcal{S}) = \int_1^{1+\langle\lambda_F-1\rangle}\int_1^{1+\langle\xi-1\rangle}\frac{C_F(\eta, \mathcal{S}_F)}{\eta}d\eta d\xi\,, \tag{4.7b}$$

where C_F is given in Eq. (4.5) and fiber along-the-chord stretch λ_F results in

$$\lambda_F = \sqrt{\mathrm{Tr}(\mathbf{CM})} = \|\mathbf{F}\,\mathbf{e}_{F,o}\|\,. \tag{4.7c}$$

Furthermore, a standard neo-Hookean approach for incompressible materials is employed for non-collagen-related strain-energy contribution Ψ_M, resulting in

$$\Psi_M(\hat{\mathbf{C}}) = k_M(\hat{I}_1 - 3)\,, \tag{4.7d}$$

with k_M being a material constant and $\hat{I}_1 = I_3^{-1/3}\mathrm{Tr}(\mathbf{C})$.

Accordingly, arterial tissue mechanical response depends on set $\mathcal{S}$ of biophysical, biochemical, and histological parameters,

$$\mathcal{S} = \{\mathcal{S}_F,\ \mathbf{e}_{F,o},\ V_C,\ V_M,\ k_M\}\,, \tag{4.8}$$

where $\mathcal{S}_F$ (defined in Eqs. (4.4)) accounts for collagen nonlinearities.

It is worth pointing out that cells in arterial tissues (i.e., SMCs) may contract and relax, affecting the *in vivo* tissue response. SMCs active contraction is here neglected, although present formulation can be straightforwardly generalized by following well-established approaches (e.g., Nardinocchi and Teresi, 2007).

4.3.3.3 *Mechanical Equilibrium*

Arterial mechanical equilibrium is associated with the solution of problem M (see Eq. (4.1)) which is here defined. In general, arterial mechanics is a fluid–structure interaction problem, with boundary conditions $\mathcal{B}_{\mathsf{M}}$ on the arterial luminal surface related to blood flow. In this work, the problem is simplified by considering stationary conditions for the fluid. Therefore, apart from possible kinematic constraints, a given uniform luminal pressure is considered, neglecting any unsteady fluid–structure interaction effects. Accordingly, boundary conditions are defined by:

$$\mathcal{B}_{\mathsf{M}}: \begin{cases} \text{a given surface traction } \hat{\mathbf{t}} \in \mathbb{R}^3 & \text{on } \Sigma_{\sigma,o}, \\ \text{a prescribed displacement } \hat{\mathbf{u}} \in \mathbb{R}^3 & \text{on } \Sigma_{u,o}, \end{cases} \tag{4.9}$$

with $\Sigma_{u,o} \cup \Sigma_{p,o} = \Sigma_o$ and with $\hat{\mathbf{t}}$ describing the assigned luminal pressure.

The Mechanical Problem M is defined as follows:

Mechanical Problem M. Find

$$\Omega = \{\mathbf{x}(X,t) \text{ with } X \in \mathcal{A},\ t \in \mathbb{R}^+\}, \qquad \mathbf{S} = \sqrt{I_3}\mathbf{F}^{-1}\boldsymbol{\sigma}\mathbf{F}^{-T},$$

such that

$$\mathrm{Div}(\mathbf{FS}) = \mathbf{0} \text{ in } \Omega_o, \text{ with } \begin{cases} \mathbf{FSn}_o = \hat{\mathbf{t}} & \text{on } \Sigma_{\sigma,o}, \\ \mathbf{u} = \hat{\mathbf{u}} & \text{on } \Sigma_{u,o}, \end{cases}$$

where $\mathbf{F} = \mathbf{I} + \mathrm{Grad}\,\mathbf{u}$ is the deformation gradient, $\mathbf{u} = \mathbf{x} - \mathbf{x}_o$ is the displacement field, and $\mathbf{S}$ is the second Piola–Kirchhoff stress tensor defined from the Cauchy stress tensor $\boldsymbol{\sigma}$ in Eq. (4.6), with $\Psi_T = \Psi_T(\mathbf{C}, \mathcal{S})$ in Eq. (4.7), $\mathbf{C} = \mathbf{F}^T\mathbf{F}$ and $I_3 = \det(\mathbf{C})$.

4.3.4 Molecular Transport Problem

The biochemical environment $\mathbf{c}$ in arterial tissue is obtained defining the Transport Problem T (see Eq. (4.2)) as an advection–diffusion–reaction problem for each active molecule q (Truskey et al., 2010). To this aim, let us introduce:

- The diffusivity $\mathbf{D}_q$ that generally results in a space dependent second-order tensor with non-negative elements and accounts for possible anisotropy effects. It can be a function of tissue microstructure (described by $\mathcal{S}$) and of the existing biochemical environment (represented by $\mathbf{c}$). Accordingly, it becomes $\mathbf{D}_q = \mathbf{D}_q(\mathbf{x}, \mathcal{S}, \mathbf{c})$;
- A reaction term $\mathfrak{R}_q$ that is split in a source term $\mathfrak{R}_q^+$ and a consumption term $\mathfrak{R}_q^-$, namely $\mathfrak{R}_q = \mathfrak{R}_q^+ - \mathfrak{R}_q^-$. These terms include possible sources, sinks, or interactions among the substances. For example, a substance can bound to cell receptor and can activate a signaling effect that acts as a source or sink for other species (see Section 4.2.3); an anomalously stretched tissue can promote or can inhibit microchannels formation, paving the way to chemical agent reactions. Accordingly, the reaction term generally depends on the existing

biochemical environment (described by $\mathbf{c}$) and on tissue strain[1] (namely, $\mathbf{C}$), resulting in $\mathfrak{R}_q^{\pm} = \mathfrak{R}_q^{\pm}(\mathbf{c}, \mathbf{C})$;

- The filtration velocity $\mathbf{v}$ that is associated with seepage. Vessel walls are indeed permeable to blood plasma, resulting in a filtration flux over the entire luminal surface, induced by the occurrence of transmural pressure gradients (Wada and Karino, 1999). As a consequence, the molecules are also transported in the vessel radial direction, with a filtration velocity that can be considered almost constant and, for physiological transmural pressure gradients, on the order of 10^{-6} cm/s (Pontrelli and De Monte, 2007; Vairo et al., 2010).

Boundary conditions are defined by

$$\mathcal{B}_{\mathsf{T}} : \begin{cases} \text{a given concentration } \hat{c}_q \in \mathbb{R}^+ & \text{on } \Sigma_c, \\ \text{a prescribed concentration flux } \hat{J}_q \in \mathbb{R} & \text{on } \Sigma_J, \\ \text{a permeable surface with permeability } \hat{\lambda}_q \in \mathbb{R}^+ & \text{on } \Sigma_r, \end{cases} \tag{4.10}$$

with $\Sigma_c \cup \Sigma_J \cup \Sigma_r = \Sigma$, and associated respectively to Dirichlet-, Neumann- and Robin-type conditions (Farlow, 1982; Tarbell, 2003). An initial concentration profile $c_q^o(\mathbf{x})$ at time $t = 0$ defines the initial condition $\mathcal{I}_{\mathsf{T}}$.

The Transport Problem T is defined as follows:

Transport Problem T. Find $c_q(\mathbf{x}, t)$ such that

$$\frac{\partial c_q}{\partial t} + \operatorname{div}(-\mathbf{D}_q(\mathbf{x}, \mathcal{S}, \mathbf{c}) \operatorname{grad} c_q + \mathbf{v} c_q) = \mathfrak{R}_q^+(\mathbf{c}, \mathbf{C}) - \mathfrak{R}_q^-(\mathbf{c}, \mathbf{C}) \text{ in } \Omega\,,$$

with $c_q(\mathbf{x}, 0) = c_q^o(\mathbf{x})$, and

$$\begin{cases} c_q(\mathbf{x}, t) = \hat{c}_q & \text{on } \Sigma_c, \\ -\mathbf{D}_q \operatorname{grad} c_q(\mathbf{x}, t) \cdot \mathbf{n} = \hat{J}_q & \text{on } \Sigma_J, \\ -\mathbf{D}_q \operatorname{grad} c_q(\mathbf{x}, t) \cdot \mathbf{n} = \hat{\lambda}_q c_q + \hat{J}_q & \text{on } \Sigma_r. \end{cases}$$

4.3.5 Remodeling Laws

The Remodeling Problem R (see Eq. (4.3)) is here presented as a non-local problem and by taking inspiration from the logistic function which finds application in a range of fields including biology, chemistry, medicine, and biomathematics (Vandermeer, 2010). To this aim, the following quantities are introduced:

- An homeostatic value for the jth structural feature, denoted by $\bar{s}_j = \bar{s}_j(\mathbf{x})$, corresponds to a set of values (collected in $\bar{\mathcal{C}}_j$) for the concentration profiles $\mathbf{c}$ not activating remodeling;

[1] Alternatively (or in conjunction), reaction terms might depend on tissue stress $\boldsymbol{\sigma}$. This is not considered in what follows, although the present approach can be straightforwardly generalized.

- The homeostatic imbalance, denoted by $\mathfrak{I}_j$, represents the imbalance from the homeostatic state induced by remodeling such that, roughly speaking, one has

$$s_j \to \bar{s}_j + \mathfrak{I}_j(\mathbf{c})\,. \tag{4.11a}$$

  The quantity $\mathfrak{I}_j$ depends on biochemical mechanisms (described by $\mathbf{c}$), resulting in $\mathfrak{I}_j = \mathfrak{I}_j(\mathbf{c})$, and it activates for non-homeostatic concentrations, namely $\mathfrak{I}_j(\mathbf{c}) = 0$ if $\mathbf{c} \in \bar{\mathcal{C}}_j$ and $\mathfrak{I}_j(\mathbf{c}) \neq 0$ if $\mathbf{c} \notin \bar{\mathcal{C}}_j$. A general expression for $\mathfrak{I}_j(\mathbf{c})$ cannot be provided because of high case-by-case variability. In fact, experimental observations (see, for instance, the ones reported in Section 4.2.3) highlight that the same structural feature can be altered in a very different way by different molecules, cell–cell signaling pathways can be involved, and biochemistry-dependent up- and down-regulations often occur. As a general rule-of-thumb and assuming an additive decomposition of the remodeling mechanisms, $\mathfrak{I}_j(\mathbf{c})$ could be defined as

$$\mathfrak{I}_j(\mathbf{c}) = \sum_{q=1}^{M} \mathfrak{i}_{qj}(c_q)\,, \tag{4.11b}$$

  with $\mathfrak{i}_{qj}(c_q)$ being the remodeling law which drives s_j as a function of c_q. For instance, a linear threshold-based activation law is obtained by defining $\mathfrak{i}_{qj}(c_q)$ as

$$\mathfrak{i}_{qj}(c_q) = \pm K^{\mathsf{R}}_{qj} \langle c_q - C^{\mathsf{R}}_{qj} \rangle \tag{4.11c}$$

  where C^{R}_{qj} is the threshold value activating remodeling, K^{R}_{qj} is a positive remodeling constant, and the sign depends on the biochemical activity (namely, it is positive if c_q induces the synthesis of s_j and negative for its degradation);
- The set $\mathcal{K}_j$ of admissible values for s_j accounts for physical constraints;
- The remodeling diffusivity $\mathbf{A}_j$ accounts for non-local and possible anisotropic effects associated with the influence area of the remodeling stimulus. In general, $\mathbf{A}_j$ is a space-dependent second-order tensor with non-negative elements and can be a function of tissue microstructure (described by $\mathcal{S}$) and biochemical environment (described by $\mathbf{c}$), namely $\mathbf{A}_j = \mathbf{A}_j(\mathbf{x}, \mathcal{S}, \mathbf{c})$;
- The remodeling viscosity $v_j \in \mathbb{R}^{++}$ accounts for the biochemical resistance to remodeling.

In general, a prescribed flux $Q_j \in \mathbb{R}$ can be imposed as a boundary condition $\mathcal{B}_{\mathsf{R}}$ on Σ in order to account for possible external agents (e.g., chemical, electromagnetical, radioactive factors) acting on the boundary surface and inducing remodeling. An initial value $s^o_j(\mathbf{x})$ at time $t = 0$ defines the initial condition $\mathcal{I}_{\mathsf{R}}$.

The Remodeling Problem R is defined as follows:

Remodeling Problem R. Find $s_j = s_j(\mathbf{x}, t) \in \mathcal{K}_j$ such that

$$\frac{\partial s_j}{\partial t} - \operatorname{div}[\mathbf{A}_j(\mathbf{x}, \mathcal{S}, \mathbf{c}) \operatorname{grad}(s_j - \bar{s}_j)] = -\left(\frac{s_j}{\bar{s}_j + \mathfrak{I}_j(\mathbf{c})} - 1\right) \frac{s_j}{v_j} \quad \text{in } \Omega\,,$$

with $s_j(\mathbf{x}, 0) = s^o_j(\mathbf{x})$ and $-\mathbf{A}_j \operatorname{grad}(s_j) \cdot \mathbf{n} = Q_j$ on Σ.

The solution of Problem R gives the implicit relationship $\mathcal{S} = \mathcal{S}(\mathbf{c})$. In particular, considering an initial homeostatic state (namely, $\mathbf{c} = \bar{\mathbf{c}}_j$ and $s_j^o = \bar{s}_j$), it is immediate to observe that R gives $s_j = \bar{s}_j$ (since $\mathcal{I}_j(\bar{\mathbf{c}}_j) = 0$). On the other hand, when $\mathbf{c} \neq \bar{\mathbf{c}}_j$, the remodeling is activated and it induces a variation of s_j.

It is worth highlighting that the description of remodeling through problem R does not allow us to consider the natural turn-over of ECM constituents but it represents an effective strategy for describing tissue pathological remodeling associated with alterations in tissue biochemical environment.

4.3.6 Integrated Computational Strategy: Towards an Analytical Solution

From the complex interplay of the afore-described ingredients, arterial multiphysics is governed by a nonlinear and strongly-coupled system of partial differential equations, resulting in a closed-loop system (see Fig. 4.2). As a matter of fact, Transport Problem T (Section 4.3.4) affects the Remodeling Problem R (Section 4.3.5) and vice versa. Moreover, remodeling mechanisms alter $\mathcal{S}$ and thus the solution of the Mechanical Problem M (Section 4.3.3) which, in turn, affects the Transport Problem T because the latter is solved in the current configuration Ω and the reaction terms $\mathfrak{R}_q^{\pm}$ depend on $\mathbf{C}$ (namely, a mechanical feedback mechanism occurs).

Rigorously, the solution of Problems M, T and R should be faced via a monolithic approach. Accordingly, the development of a solution strategy for arterial multiphysics is not a trivial task. Nevertheless, it is worth highlighting that, due to arterial adaptation processes, remodeling laws are characterized by large time scales (i.e., months to years) which can be believed to be significantly higher than the ones of microscale transport (i.e., hours to days) and of arterial mechanics (i.e., seconds due to the characteristic times of the cardiac cycle).

Taking advantage of the separation of time scales, Problem i (with $i = \mathsf{M}, \mathsf{T}, \mathsf{R}$) can be solved by considering its own time-variable t_i and a characteristic time T_i in which the solution of Problem i attains a steady-state, with $T_{\mathsf{R}} \gg T_{\mathsf{T}} \gg T_{\mathsf{M}}$. Accordingly, the principle of separation of time-scales might be exploited for obtaining an effective solution strategy. Nevertheless, a solution strategy for the fully-coupled formulation is beyond the scope of present work. Here a number of simplifying assumptions are introduced in order to move towards a quasi-analytical solution strategy and to show the effectiveness of the present approach. In detail, the following assumptions are considered:

1. $\mathbf{D}_q$ in T does not depend on tissue microstructure $\mathcal{S}$;
2. $\mathfrak{R}_q^{\pm}$ in T does not depend on $\mathbf{C}$ (i.e., no mechanical feedback is accounted for);
3. T is solved on the arterial configuration $\bar{\Omega}$ corresponding to the homeostatic state, associated with $\bar{\mathcal{S}} = \{\bar{s}_1, \dots, \bar{s}_S\}$;
4. R is solved assuming that remodeling is a local phenomenon (namely, $\mathbf{A}_j = \mathbf{0}$);
5. Since $T_{\mathsf{R}} \gg T_{\mathsf{T}}$, R is solved employing steady-state concentration profiles $\tilde{\mathbf{c}}(\mathbf{x}) = (\tilde{c}_1(\mathbf{x}) \dots \tilde{c}_M(\mathbf{x}))$;

In agreement with previous assumptions, Reduced Transport $\tilde{\mathsf{T}}$ and Remodeling $\tilde{\mathsf{R}}$ Problems are introduced such that

$$\tilde{\mathbf{c}}(\mathbf{x}) = \tilde{\mathsf{T}}(\bar{\Omega}, \mathcal{B}_{\mathsf{T}}), \qquad \mathcal{S}(\mathbf{x}, t) = \tilde{\mathsf{R}}(\tilde{\mathbf{c}}(\mathbf{x}), \mathcal{I}_{\mathsf{R}}). \tag{4.12}$$

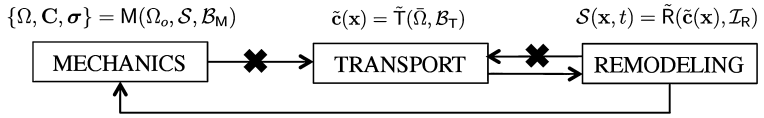

FIGURE 4.4 Arterial multiphysics modeling: the fully-coupled system reduces to the open-loop one by neglecting the mechanical feedback on molecular transport (crossed right-oriented arrow) and the dependence of the transport on the remodeling (crossed left-oriented arrow) obtained from the fully-coupled system.

Problems $\tilde{\mathsf{T}}$ and $\tilde{\mathsf{R}}$ are defined as follows:

Reduced Transport Problem $\tilde{\mathsf{T}}$. Find $\tilde{c}_q(\mathbf{x})$ such that

$$\operatorname{div}(-\mathbf{D}_q(\mathbf{x}, \tilde{\mathbf{c}}) \operatorname{grad} \tilde{c}_q + \mathbf{v}\tilde{c}_q) = \mathfrak{R}_q^+(\tilde{\mathbf{c}}) - \mathfrak{R}_q^-(\tilde{\mathbf{c}}) \quad \text{in } \bar{\Omega}$$

with

$$\begin{cases} \tilde{c}_q(\mathbf{x}) = \hat{c}_q & \text{on } \bar{\Sigma}_c, \\ -\mathbf{D}_q \operatorname{grad} \tilde{c}_q(\mathbf{x}) \cdot \mathbf{n} = \hat{J}_q & \text{on } \bar{\Sigma}_J, \\ -\mathbf{D}_q \operatorname{grad} \tilde{c}_q(\mathbf{x}) \cdot \mathbf{n} = \hat{\lambda}_q \tilde{c}_q(\mathbf{x}) + \hat{J}_q & \text{on } \bar{\Sigma}_r. \end{cases}$$

Reduced Remodeling Problem $\tilde{\mathsf{R}}$. Find $s_j = s_j(\mathbf{x}, t) \in \mathcal{K}_j$ such that

$$\frac{\partial s_j}{\partial t} = -\left(\frac{s_j}{\bar{s}_j + \mathfrak{I}_j(\tilde{\mathbf{c}})} - 1\right) \frac{s_j}{\nu_j},$$

with $s_j(\mathbf{x}, 0) = s_j^o(\mathbf{x})$.

It is worth pointing out that, assuming $\mathcal{K}_j \equiv \mathbb{R}$, problem $\tilde{\mathsf{R}}$ can be solved in an analytical way, obtaining

$$s_j(\mathbf{x}, t) = \frac{s_j^o(\mathbf{x})[\bar{s}_j(\mathbf{x}) + \mathfrak{I}_j(\tilde{\mathbf{c}})] \exp(t/\nu_j)}{\bar{s}_j(\mathbf{x}) + \mathfrak{I}_j(\tilde{\mathbf{c}}) + s_j^o(\mathbf{x})[\exp(t/\nu_j) - 1]}, \tag{4.13a}$$

where it is immediate to verify that

$$\lim_{t \to +\infty} s_j(\mathbf{x}, t) = \bar{s}_j(\mathbf{x}) + \mathfrak{I}_j(\tilde{\mathbf{c}}). \tag{4.13b}$$

Accordingly, under the afore-introduced assumptions, M does not affect the solution of T and R (apart from the computation of the homeostatic configuration). Clearly, the solution of T affects R which, in turn, affects M. As schematically depicted in Fig. 4.4, an open-loop multiphysics system is obtained, opening to the investigation of the effects of biochemical processes on mechanics but not vice versa.

In this case, open-loop arterial multiphysics can be obtained from the pseudocode in Table 4.1. The proposed solution strategy opens a way to develop analytical solutions, which allow the implementation of extensive parametric analyses aiming to furnish insights into the effects of pathological/healing biochemical stimuli on arterial mechanics. This is the aim of the case study addressed in the following Section 4.4.

TABLE 4.1 Pseudocode of the algorithm for open-loop arterial multiphysics

1. $\{\bar{\Omega}, \bar{\mathbf{C}}, \bar{\boldsymbol{\sigma}}\} = \mathsf{M}(\Omega_o, \bar{\mathcal{S}}(\mathbf{x}), \mathcal{B}_{\mathsf{M}})$,
2. $\tilde{\mathbf{c}}(\mathbf{x}) = \tilde{\mathsf{T}}(\bar{\Omega}, \mathcal{B}_{\mathsf{T}})$,
3. $\mathcal{S}(\mathbf{x}, t) = \tilde{\mathsf{R}}(\tilde{\mathbf{c}}(\mathbf{x}), \mathcal{I}_{\mathsf{R}})$,
4. $\{\Omega(t), \mathbf{C}(\mathbf{x}, t), \boldsymbol{\sigma}(\mathbf{x}, t)\} = \mathsf{M}(\Omega_o, \mathcal{S}(\mathbf{x}, t), \mathcal{B}_{\mathsf{M}})$.

4.4 AN AXISYMMETRIC CASE STUDY

In agreement with the evidence in Section 4.2.3, a model for the physiopathological control system involved on ECM remodeling in aortic tissues is described in what follows, by addressing the effects of microscale transport phenomena of MMPs (produced by SMCs in the media), TGF-β (produced by endothelial cells in the inner intima), and IL (produced by macrophages in the outer adventitia) on the aortic response.

Only the media layer is addressed, since it is the most important from the mechanical point of view. Under axisymmetrical geometric assumptions, the arterial segment (characterized by internal and external radii r_i and r_e, respectively) is loaded by a uniform internal pressure P_i. The effects of ECM remodeling mechanisms on arterial compliance is analyzed, by obtaining the pressure–radius relationship of arterial segments associated with the transport and the biochemical activity of MMPs, TGF-β and ILs which alter, as structural features: elastin and collagen volume fractions (V_{EL} and V_C), collagen fiber radius (r_F), inter-molecular cross-links density (Λ_c), and fiber orientation distribution (see Fig. 4.5). In the following, subscript a takes values in $\{2, 3\}$, q in $\{1, 2, 3\}$, and j in $\{1, \ldots, S\}$.

4.4.1 Arterial Geometry and Structure

A single-layer thick-walled right cylinder (L_a long) is addressed, modeling the media layer of an aortic segment. By following the opening angle method (see Fig. 4.5) and denoting by α the opening angle (Auricchio et al., 2014; Holzapfel et al., 2000), the material points in the reference configuration Ω_o (assumed to be load-free and stress-free) are identified by the cylindrical coordinates $\mathbf{x}_o = (r_o, \theta_o, z_o)$ where

$$r_{i,o} \leq r_o \leq r_{e,o}\,, \quad 0 \leq \theta_o \leq 2\pi - \alpha\,, \quad 0 \leq z_o \leq L_{a,o}\,, \tag{4.14a}$$

for the radial, circumferential, and axial coordinate, respectively. On the other hand, the current configuration Ω is described by the cylindrical coordinates $\mathbf{x} = (r, \theta, z)$ where

$$r_i \leq r \leq r_e\,, \qquad 0 \leq \theta \leq 2\pi\,, \qquad 0 \leq z \leq L_a\,. \tag{4.14b}$$

Introducing $\kappa = 2\pi/(2\pi - \alpha)$ and λ_z as a constant axial stretch, function $\mathbf{x} = \mathbf{x}(\mathbf{x}_o)$ results in

$$r = r(r_o) = \sqrt{\frac{r_o^2 - r_{i,o}^2}{\kappa\lambda_z} + r_i^2}\,, \quad \theta = \theta(\theta_o) = \kappa\theta_o\,, \quad z = z(z_o) = \lambda_z z_o\,, \tag{4.14c}$$

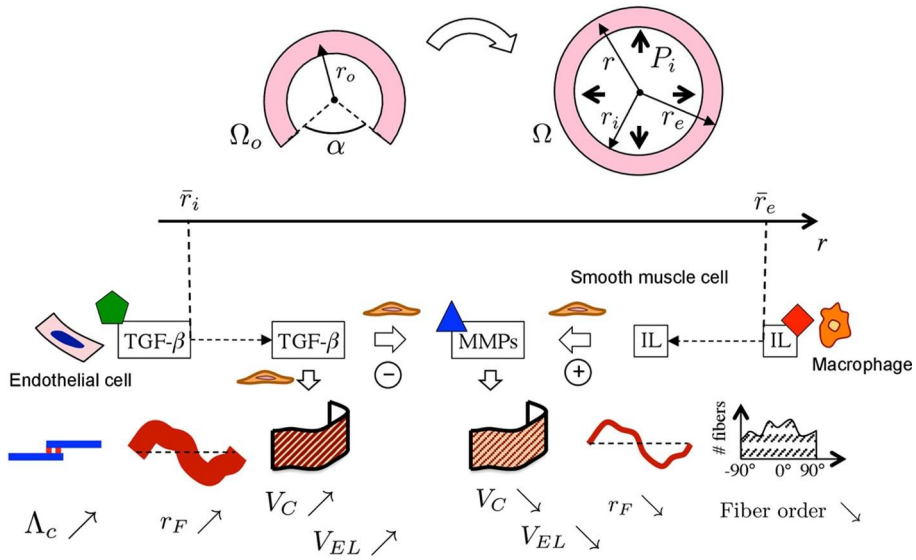

FIGURE 4.5 Axisymmetric case study for arterial multiphysics. Reference (with opening angle α and radial coordinate r_o) and current configuration (with radial coordinate r, internal and external radius r_i and r_e, and luminal pressure P_i). It is sketched the transport of matrix metalloproteinases (MMPs), transforming growth factor-beta (TGF-β), interleukines (ILs), the remodeling of elastin and collagen volume fractions (V_{EL} and V_C), collagen fiber radius (r_F), inter-molecular cross-links density (Λ_c), and fiber orientation distribution.

due to the incompressibility condition. The inverse function $r_o(r)$ can be also straightforwardly defined as

$$r_o = r_o(r) = \sqrt{\kappa \lambda_z (r^2 - r_i^2) + r_{i,o}^2}\,. \tag{4.14d}$$

Moreover, the deformation gradient expressed in the cylindrical coordinate system results in

$$\mathbf{F} = \frac{\partial \mathbf{x}}{\partial \mathbf{x}_o} = \mathrm{diag}[\lambda_r,\, \lambda_\theta,\, \lambda_z] = \mathrm{diag}\left[\frac{\partial r}{\partial r_o},\, \frac{r}{r_o}\frac{\partial \theta}{\partial \theta_o},\, \frac{\partial z}{\partial z_o}\right] \tag{4.15a}$$

with

$$\lambda_r = \lambda_r(r) = \frac{r_o(r)}{\kappa \lambda_z r}\,, \qquad \lambda_\theta = \lambda_\theta(r) = \frac{\kappa\, r}{r_o(r)}\,. \tag{4.15b}$$

Moreover, introducing $\boldsymbol{\theta}$ and $\mathbf{z}$ as the unit vectors in the circumferential and axial direction, respectively, the unit vector identifying the direction of collagen fibers is described by

$$\mathbf{e}_F = \cos\beta\, \boldsymbol{\theta} + \sin\beta\, \mathbf{z}\,, \tag{4.16a}$$

where β represents collagen fiber angle in the current configuration with respect to the circumferential direction. Accordingly, from Eq. (4.7c), one has

$$\lambda_F = \sqrt{\lambda_\theta^2 \cos^2\beta_o + \lambda_z^2 \sin^2\beta_o}\,, \tag{4.16b}$$

where β_o represents the angle of collagen fibers in the reference configuration.

Addressing arterial microstructure (see Section 4.2.1), media lamellar units (MLUs) are explicitly considered and each MLU is regarded as made up of a thick elastin sub-layer and a composite interlamellar substance with elastin and collagen fibers (see Appendix B for a detailed description). In order to account for the heterogeneous lamellar structure of aortic media layer and for remodeling mechanisms, structural features $\mathcal{S}$ in Eq. (4.8) are assumed to vary on the radial coordinate r only, namely $\mathcal{S} = \mathcal{S}(r,t)$.

As a model assumption, structural features $\mathcal{S}_{\mathsf{R}} = \{V_{EL}, V_C, r_F, \Lambda_c, \beta_o\} \subset \mathcal{S}$ are assumed to undergo remodeling, while the remaining model parameters $\mathcal{S}_{\mathsf{NR}} = \mathcal{S} \setminus \mathcal{S}_{\mathsf{R}}$ are assumed to be constant in time.

4.4.2 Quasi-Analytical Arterial Mechanics

Under the afore-introduced assumptions on arterial geometry and microstructure, the solution of Problem M in Section 4.3.3 becomes axisymmetric and it can be solved through simple analytical relationships. In particular, arterial configuration is fully described by the line segment connecting internal and external radii, namely $\Omega \equiv [r_i, r_e]$. Moreover, Cauchy stresses σ_r and σ_θ (respectively in the radial and circumferential directions) and the luminal pressure P_i have to satisfy the following equilibrium equation:

$$P_i = \int_{r_i}^{r_e} \frac{\sigma_\theta - \sigma_r}{r}\, dr = \int_{r_i}^{r_e} \left[\lambda_\theta \frac{\partial \Psi_T}{\partial \lambda_\theta} - \lambda_r \frac{\partial \Psi_T}{\partial \lambda_r}\right] \frac{dr}{r}\,. \tag{4.17a}$$

Here Eq. (4.6) has been accounted for, and the Lagrange multiplier p has been straightforwardly eliminated due to the appearance of stress difference $\sigma_\theta - \sigma_r$. Accounting for Eq. (4.16b) and referring to the constitutive model in Eqs. (4.7), we obtain

$$\frac{\partial \Psi_T}{\partial \lambda_r} = V_M \frac{\partial \Psi_M}{\partial \lambda_r} + \frac{\partial \lambda_F}{\partial \lambda_r} V_C \int_1^{1+\langle \lambda_F - 1\rangle} \frac{C_F(\eta, \mathcal{S}_F)}{\eta}\, d\eta = V_M \frac{\partial \Psi_M}{\partial \lambda_r}\,, \tag{4.17b}$$

$$\begin{aligned} \frac{\partial \Psi_T}{\partial \lambda_\theta} &= V_M \frac{\partial \Psi_M}{\partial \lambda_\theta} + \frac{\partial \lambda_F}{\partial \lambda_\theta} V_C \int_1^{1+\langle \lambda_F - 1\rangle} \frac{C_F(\eta, \mathcal{S}_F)}{\eta}\, d\eta = \\ &= V_M \frac{\partial \Psi_M}{\partial \lambda_\theta} + V_C \frac{\lambda_\theta \cos^2\beta_o}{\lambda_F} \int_1^{1+\langle \lambda_F - 1\rangle} \frac{C_F(\eta, \mathcal{S}_F)}{\eta}\, d\eta\,. \end{aligned} \tag{4.17c}$$

Accordingly, Eqs. (4.17) provide the quasi-analytical relationship

$$P_i = P_i(r_i, \mathcal{S}(r,t))\,. \tag{4.18}$$

Therefore, the homeostatic state can be computed as

$$\bar{\Omega} \equiv [\bar{r}_i, \bar{r}_e] \;\text{ s.t. }\; P_i(\bar{r}_i, \bar{\mathcal{S}}) = \bar{P}_i\,, \tag{4.19}$$

where $\bar{P}_i$ represent a stationary physiological pressure.

4.4.3 Analytical Arterial Molecular Transport

Let c_1, c_2, and c_3 respectively denote the concentrations of MMPs, TGF-β, and IL, where

- IL activates the synthesis of MMPs by SMCs;
- TGF-β inhibits the synthesis of MMPs by SMCs.[2]

The steady-state (axisymmetric) concentration profiles $\tilde{c}_q = \tilde{c}_q(r)$ are obtained from the Reduced Transport Problem $\tilde{\mathsf{T}}$ (Section 4.3.6) by assuming an isotropic diffusion with constant diffusivity (namely, $\mathbf{D}_q = \hat{D}_q \mathbf{I}$). Moreover, curvature effects and convective-terms are neglected. Furthermore, nontrivial reaction terms are defined as:

$$\mathfrak{R}_1^+(\tilde{\mathbf{c}}) = \eta_1 V_S \, R^+(\tilde{c}_3)\,(C_1 - \tilde{c}_1)\,, \tag{4.20a}$$

$$\mathfrak{R}_1^-(\tilde{\mathbf{c}}) = [\zeta_1 + \xi_1 V_S \, R^-(\tilde{c}_2)]\tilde{c}_1\,, \tag{4.20b}$$

$$\mathfrak{R}_a^-(\tilde{\mathbf{c}}) = \zeta_a \, \tilde{c}_a\,, \tag{4.20c}$$

where

- $V_S \in [0,1]$ is the volume fraction of smooth muscle cells (SMCs), assumed to be constant in time and space;
- $R^+(\tilde{c}_3)$ (resp., $R^-(\tilde{c}_2)$) is MMPs source (resp., consumption) dimensionless function, activated by the molecular species IL (resp., TGF-β) through SMCs. Simple linear expressions are herein employed, by assuming a dependence on the average concentration within the media layer, namely $R^{\pm}(\tilde{c}_a) = \tilde{c}_a^{av}/\gamma_a$, $\tilde{c}_a^{av}$ being

$$\tilde{c}_a^{av} = \frac{1}{\bar{r}_e - \bar{r}_i} \int_{\bar{r}_i}^{\bar{r}_e} \tilde{c}_a(r)\, dr\,, \tag{4.21}$$

  and γ_a representing a reference concentration value corresponding to a unitary stimulus;
- C_1 is the saturation limit of MMPs production by SMCs;
- η_1 (resp., ξ_1) is MMPs source (resp., consumption) rate mediated by SMCs;
- ζ_q are MMPs/TGF-β/IL consumption rates associated with molecular natural decay.

Accordingly, introducing $\rho \in [0,1]$ as the normalized radial coordinate $\rho = (r - \bar{r}_i)/\bar{\delta}$ with $\bar{\delta} = \bar{r}_e - \bar{r}_i$, the Reduced Transport Problem $\tilde{\mathsf{T}}$ (Section 4.3.6) reads: find $\tilde{c}_1$, $\tilde{c}_2$, and $\tilde{c}_3$ such that

$$\frac{\partial^2 \tilde{c}_1}{\partial \rho^2} + B - h_1^2 \tilde{c}_1 = 0\,, \tag{4.22a}$$

$$\frac{\partial^2 \tilde{c}_a}{\partial \rho^2} - h_a^2 \tilde{c}_a = 0\,, \tag{4.22b}$$

[2] It is worth pointing out that TGF-β promotes the synthesis of TIMPs which, in turn, reduce the activity of MMPs. In the present model, TIMPs are not explicitly modeled but their effect is taken into account by introducing a negative feedback of MMPs synthesis activated by TGF-β.

in $\rho \in [0, 1]$, with

$$B = \eta_1 \bar{\delta}^2 \frac{V_S \tilde{c}_3^{av} C_1}{\hat{D}_1 \gamma_3}, \tag{4.22c}$$

$$h_1^2 = \frac{\bar{\delta}^2}{\hat{D}_1} \left(\zeta_1 + \xi_1 \frac{V_S \tilde{c}_2^{av}}{\gamma_2} + \eta_1 \frac{V_S \tilde{c}_3^{av}}{\gamma_3} \right), \tag{4.22d}$$

$$h_a^2 = \frac{\bar{\delta}^2 \zeta_a}{\hat{D}_a}. \tag{4.22e}$$

The solution of Eqs. (4.22) can be obtained analytically: firstly, the independent Eqs. (4.22b) are solved and $\tilde{c}_a^{av}$ are computed; then, average concentrations $\tilde{c}_a^{av}$ are employed for obtaining the solution of Eq. (4.22a). Accordingly, it results in

$$\tilde{c}_1(\rho) = k_{11} \exp(-h_1 \rho) + k_{21} \exp(h_1 \rho) + \frac{B}{h_1^2}, \tag{4.23a}$$

$$\tilde{c}_a(\rho) = k_{1a} \exp(-h_a \rho) + k_{2a} \exp(h_a \rho), \tag{4.23b}$$

where constants k_{1q} and k_{2q} can be determined from boundary conditions $\mathcal{B}_\mathsf{T}$. The latter are assumed to be of Robin-type, except for Dirichlet boundary conditions at the intima-media layer for $\tilde{c}_2$ and at the media-adventitia layer for $\tilde{c}_3$, in order to respectively account for (see Section 4.2.2 and Fig. 4.5):

- A constant source of TGF-β by endothelial cells in the intima;
- A constant source of IL by macrophages in the adventitia.

Accordingly,

$$\text{at } \rho = 0 \quad \begin{cases} \dfrac{\partial \tilde{c}_1}{\partial \rho} = \dfrac{\bar{\delta} \hat{\lambda}_{1i}}{\hat{D}_1} \tilde{c}_1, \\ \tilde{c}_2 = \hat{c}_2, \\ \dfrac{\partial \tilde{c}_3}{\partial \rho} = \dfrac{\bar{\delta} \hat{\lambda}_{3i}}{\hat{D}_3} \tilde{c}_3, \end{cases} \qquad \text{at } \rho = 1 \quad \begin{cases} \dfrac{\partial \tilde{c}_1}{\partial \rho} = -\dfrac{\bar{\delta} \hat{\lambda}_{1e}}{\hat{D}_1} \tilde{c}_1, \\ \dfrac{\partial \tilde{c}_2}{\partial \rho} = -\dfrac{\bar{\delta} \hat{\lambda}_{2e}}{\hat{D}_2} \tilde{c}_2, \\ \tilde{c}_3 = \hat{c}_3. \end{cases} \tag{4.23c}$$

4.4.4 Analytical Arterial Remodeling Induced by MMPs, TGF-β, and IL

The remodeling laws are formulated by defining the homeostatic imbalance $\mathfrak{I}_j$ in the Remodeling Problem R (Section 4.3.5). As general assumptions, local remodeling is addressed (namely, $\mathbf{A}_j = \mathbf{0}$) and an additive decomposition of remodeling mechanisms based on threshold-based activation laws is employed, analogously to the form of Eqs. (4.11b) and (4.11c).

Remodeling laws are defined in agreement with the evidence in Section 4.2.3 and as schematically depicted in Fig. 4.5, accounting for the activity by MMPs ($q = 1$) and TGF-β ($q = 2$). To this aim, let constants $C_{qj}^\mathsf{R} = C_\mathsf{R}$, $K_{1j}^\mathsf{R} = \bar{s}_j / C_\mathsf{R}$, and $K_{2j}^\mathsf{R} = \bar{s}_j V_S / C_\mathsf{R}$ be introduced, where $C_\mathsf{R} \in \mathbb{R}^{++}$ is a given concentration value. It is highlighted that volume fraction V_S is accounted for in K_{2j}^R, since TGF-β activity is mediated by SMCs. Accordingly,

- Elastin volume fraction $s_1 = V_{EL}$, collagen volume fraction $s_2 = V_C$ and collagen fiber radius $s_3 = r_F$ increase with TGF-β and decrease with MMPs:

$$\mathfrak{I}_1(c_1, c_2) = \bar{V}_{EL}\,[V_S\langle c_2 - C_\mathsf{R}\rangle - \langle c_1 - C_\mathsf{R}\rangle]\,/C_\mathsf{R}\,, \tag{4.24a}$$

$$\mathfrak{I}_2(c_1, c_2) = \bar{V}_C\,[V_S\langle c_2 - C_\mathsf{R}\rangle - \langle c_1 - C_\mathsf{R}\rangle]\,/C_\mathsf{R}\,, \tag{4.24b}$$

$$\mathfrak{I}_3(c_1, c_2) = \bar{r}_F\,[V_S\langle c_2 - C_\mathsf{R}\rangle - \langle c_1 - C_\mathsf{R}\rangle]\,/C_\mathsf{R}\,; \tag{4.24c}$$

- Inter-molecular cross-link density $s_4 = \Lambda_c$ increases with TGF-β:

$$\mathfrak{I}_4(c_2) = \bar{\Lambda}_c V_S\langle c_2 - C_\mathsf{R}\rangle/C_\mathsf{R}\,; \tag{4.24d}$$

- Collagen fiber angle $s_5 = \beta_o$ tends to an isotropically distributed pattern (namely, without any preferred direction) in the presence of MMPs:

$$\mathfrak{I}_5(c_1) = (\beta_{iso} - \bar{\beta}_o)\,f_h(c_1 - C_\mathsf{R})\,, \tag{4.24e}$$

  where $\beta_{iso} = \beta_{iso}(r)$ corresponds to an isotropic angle distribution (see Eq. (B.2) in Appendix B), and $f_h(x)$ is the Heaviside function (i.e., $f_h(x) = 0$ for $x \leq 0$ and $f_h(x) = 1$ for $x > 0$).

Let the homeostatic state be assumed as an initial condition and let ν be a remodeling viscosity, constant among different structural features (namely, $s_j^o = \bar{s}_j$ and $\nu_j = \nu$). Employing steady-state concentration profiles $\tilde{c}_1$ and $\tilde{c}_2$ in Eqs. (4.23), the Remodeling Problem corresponds to its Reduced form $\tilde{\mathsf{R}}$ (Section 4.3.6). Accounting for Eqs. (4.24), analytical solutions for ECM remodeling in arterial tissues of the form of Eqs. (4.13) directly follow as:

$$V_{EL}(r,t) = \frac{\bar{V}_{EL}\left[C_\mathsf{R} + V_S\langle\tilde{c}_2(r) - C_\mathsf{R}\rangle - \langle\tilde{c}_1(r) - C_\mathsf{R}\rangle\right]}{C_\mathsf{R} + \left[V_S\langle\tilde{c}_2(r) - C_\mathsf{R}\rangle - \langle\tilde{c}_1(r) - C_\mathsf{R}\rangle\right]\exp(-t/\nu)}, \tag{4.25a}$$

$$V_C(r,t) = \frac{\bar{V}_C\left[C_\mathsf{R} + V_S\langle\tilde{c}_2(r) - C_\mathsf{R}\rangle - \langle\tilde{c}_1(r) - C_\mathsf{R}\rangle\right]}{C_\mathsf{R} + \left[V_S\langle\tilde{c}_2(r) - C_\mathsf{R}\rangle - \langle\tilde{c}_1(r) - C_\mathsf{R}\rangle\right]\exp(-t/\nu)}, \tag{4.25b}$$

$$r_F(r,t) = \frac{\bar{r}_F\left[C_\mathsf{R} + V_S\langle\tilde{c}_2(r) - C_\mathsf{R}\rangle - \langle\tilde{c}_1(r) - C_\mathsf{R}\rangle\right]}{C_\mathsf{R} + \left[V_S\langle\tilde{c}_2(r) - C_\mathsf{R}\rangle - \langle\tilde{c}_1(r) - C_\mathsf{R}\rangle\right]\exp(-t/\nu)}, \tag{4.25c}$$

$$\Lambda_c(r,t) = \frac{\bar{\Lambda}_c\left[C_\mathsf{R} + V_S\langle\tilde{c}_2(r) - C_\mathsf{R}\rangle\right]}{C_\mathsf{R} + V_S\langle\tilde{c}_2(r) - C_\mathsf{R}\rangle\exp(-t/\nu)}, \tag{4.25d}$$

$$\beta_o(r,t) = \frac{\bar{\beta}_o(r)\left[\bar{\beta}_o(r) + (\beta_{iso}(r) - \bar{\beta}_o(r))\,f_h(\tilde{c}_1(r) - C_\mathsf{R})\right]}{\bar{\beta}_o(r) + [\beta_{iso}(r) - \bar{\beta}_o(r)]\,f_h(\tilde{c}_1(r) - C_\mathsf{R})\exp(-t/\nu)}\,. \tag{4.25e}$$

From Eq. (4.25a), the volume fraction of non-collagenous matrix $V_M(r,t) = V_{EL}(r,t) + V_S$ is obtained. Moreover, from both Eqs. (4.25a) and (4.25b), the volume fraction of non-bearing-load constituents (i.e., fragmented elastin and degraded collagen) is obtained as $V_0(r,t) = 1 - (V_C(r,t) + V_{EL}(r,t) + V_S)$. For defining the admissible set of values $\mathcal{K}_j$, physical constraints $V_C(r,t) \geq 0$, $V_{EL}(r,t) \geq 0$ and $V_0(r,t) \geq 0$ (or equivalently, $V_C(r,t) + V_{EL}(r,t) \leq 1 - V_S$) are employed as lower and upper bound limits for Eqs. (4.25a) and (4.25b), as well as $r_F(r,t) \geq 0$ for Eq. (4.25c) and $\Lambda_c(r,t) \geq 0$ for Eq. (4.25d).

TABLE 4.2 Pseudocode of the algorithm for quasi-analytical arterial multiphysics

1. Find $[\bar{r}_i, \bar{r}_e]$ from Eq. (4.19),
2. Find $\{\tilde{c}_1, \tilde{c}_2, \tilde{c}_3\}$ from Eqs. (4.23),
3. Find $\mathcal{S}(r,t)$ from Eqs. (4.25),
4. Find $P_i(r_i, \mathcal{S}(r,t))$ from Eq. (4.18).

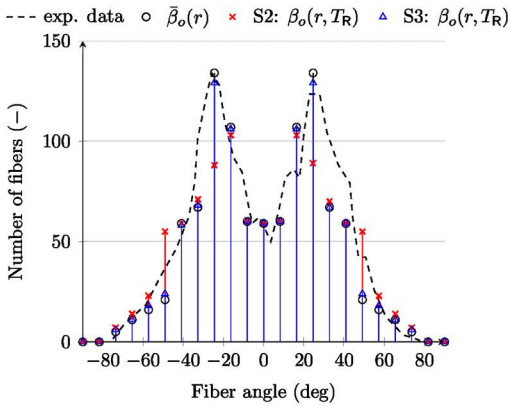

FIGURE 4.6 Total number of collagen fibers for different fiber angles: homeostatic $\bar{\beta}_o(r)$ and remodeled distributions at steady-state $\beta_o(r, T_R)$ for scenarios S2 and S3, compared with experimental data by Schriefl et al. (2012). Values of parameters in Tables 4.3 and 4.4.

To evaluate the characteristic remodeling time interval T_R (namely, the time interval to reach a steady state), let $\epsilon \ll 1$ be an arbitrary positive constant and, in agreement with Eq. (4.13b), define T_R such that $s_j(r, T_R) = \bar{s}_j + \mathfrak{I}_j \approx (1-\epsilon)(\bar{s}_j + \mathfrak{I}_j)$. Accordingly, from Eqs. (4.25) and assuming $\mathfrak{I}_j \propto \bar{s}_j$, T_R can be estimated as:

$$T_R = \nu \log\left(\frac{(1-\epsilon)\mathfrak{I}_j}{\epsilon\, \bar{s}_j}\right) \approx \nu \log\left(\frac{1-\epsilon}{\epsilon}\right). \tag{4.26}$$

4.4.5 Results

In the line of the solution strategy introduced in Section 4.3.6 and Table 4.1, numerical results are obtained by adopting the procedure in the pseudocode of Table 4.2. Addressing arterial media layer only, the model is parameterized for a thoracic aortic segment. It is worth highlighting that well-established experimental data (Buehler and Wong, 2007; Clark and Glagov, 1985; O'Connell et al., 2008; Marino and Vairo, 2013, 2014; Marino, 2016; Schriefl et al., 2012) are available for setting the values of model parameters describing the homeostatic state $\bar{\mathcal{S}}$, which is assumed as corresponding to the initial state (namely, at $t = 0$). In the following simulations, values in Table 4.3 are employed for model parameters at homeostasis. For instance, addressing fiber orientation distribution, Fig. 4.6 shows a comparison between model setting and histological measurements.

TABLE 4.3 Values of structural parameters defining reference geometry ($r_{i,o}$, $r_{e,o}$, and α) and the homeostatic state $\bar{\mathcal{S}}$ in agreement with data by Auricchio et al. (2014), Buehler and Wong (2007), Clark and Glagov (1985), O'Connell et al. (2008), Holzapfel and Ogden (2010), Marino and Vairo (2013, 2014), Marino (2016), Schriefl et al. (2012) and with the microstructure model in Appendix B (the bar symbol is omitted for parameters not undergoing remodeling). Arterial tissue comprises N_M media lamellar units (MLUs) along its thickness, and each MLU is divided in n_M sub-layers. MLUs and sub-layers are assumed to be identical in thickness. Within each sub-layer, $s_j \in \mathcal{S}$ is piecewise constant and, if variable across arterial thickness, defined by the value at $r = r^{k,p}$, representing the middle position of the pth sub-layer in the kth MLU. In the table, $k \in \{1, \dots, N_M\}$ and $c \in \{2, \dots, n_M\}$

Parameter	Value (with unit of measure)	Definition
$r_{i,o}$	8.24 mm	Arterial internal radius (in Ω_o)
$r_{e,o}$	9.14 mm	Arterial external radius (in Ω_o)
α	80°	Arterial opening angle
N_M	60	Number of Media Lamellar Units (MLUs)
n_M	18	Number of sub-layers in each MLU
$\bar{V}_{EL} = \bar{V}_{EL}(r)$	$\begin{cases} 0.5 & \text{for } r = r^{k,1} \\ 0.36 & \text{for } r = r^{k,c} \end{cases}$	Elastin volume fraction
$\bar{V}_C = \bar{V}_C(r)$	$\begin{cases} 0 & \text{for } r = r^{k,1} \\ 0.14 & \text{for } r = r^{k,c} \end{cases}$	Collagen volume fraction
V_S	0.2	Volume fraction of smooth muscle cells
$\bar{r}_F$	0.5 µm	Collagen fiber radius
$H_{F,o}$	1.3 µm	Collagen fiber amplitude (in Ω_o)
$L_{F,o}$	5 µm	Collagen fiber period (in Ω_o)
$\bar{\beta}_o = \bar{\beta}_o(r)$	Eqs. (B.1) with $\hat{\beta} = 25°$	Collagen fiber angle (in Ω_o)
$\bar{\Lambda}_c$	1 mol/mol	Inter-molecular cross-links density
k_c	105 nN/µm	Inter-molecular cross-links stiffness
$\ell_{m,o}$	279 nm	Molecular end-to-end length (in Ω_o)
ℓ_c	287 nm	Molecular contour length
ℓ_p	14.5 nm	Molecular persistence length
T	37°C	Body temperature
A_m	1.41 nm^2	Molecular cross-sectional area
$\hat{E}_o$	1 GPa	Low-strain triple-helix tangent modulus
$\hat{E}$	80 GPa	High-strain triple-helix tangent modulus
η	22.5	Triple-helix uncoiling resistance
ε_o^h	0.1	Triple-helix uncoiling strain
k_M	2.2 MPa	Elastin stiffness

As shown in Fig. 4.7, the obtained pressure–radius relationship $P_i(r_i, \bar{\mathcal{S}})$ is reported, clearly showing that it fully agrees with available experimental data (Hallock and Benson, 1937) and proving the effectiveness of present approach in capturing a realistic mechanical behavior of thoracic aortic segments. Moreover, by choosing $\bar{P}_i = 100$ mm Hg as reference physiological pressure, the initialization step (step 1 in Table 4.2) gives:

$$\bar{r}_i = 9.1\,\text{mm}\,, \qquad \bar{r}_e = 9.74\,\text{mm}\,. \tag{4.27}$$

Addressing transport-remodeling phenomena, let $\hat{c}$ denote a basal molecular production (assumed to be constant among different molecules for the sake of simplicity) and let $\gamma_a =$

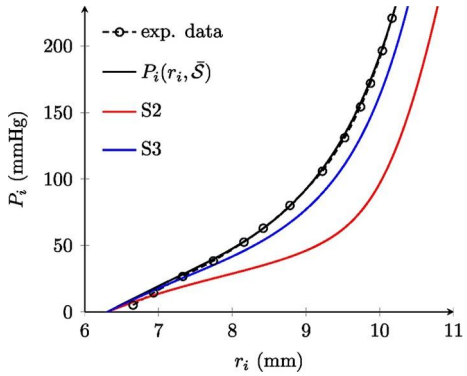

FIGURE 4.7 Pressure–radius relationship $P_i(r_i, \bar{\mathcal{S}})$ (corresponding to the one obtained in scenario S1) and $P_i(r_i, \mathcal{S}(r, T_R))$ for scenarios S2 and S3 (at steady-state), compared with experimental data by Hallock and Benson (1937). Values of parameters in Tables 4.3 and 4.4.

TABLE 4.4 Values of parameters for the transport-remodeling problems in the axisymmetric arterial study case, with $\hat{D}_q = \hat{D}$, $\zeta_q = \zeta$, and $\hat{\lambda}_{qi} = \hat{\lambda}_{qe} = \hat{\lambda}$ in Eqs. (4.23). With reference to Eq. (4.26), ratio $\nu / T_R = 0.1$ ensures $\epsilon < 10^{-4}$

Parameter	$\hat{D}$	ζ	η_1	ξ_1	$\hat{\lambda}$	ν	T_R
Unit of measurement	$\text{mm}^2\,\text{s}^{-1}$	s^{-1}	s^{-1}	s^{-1}	$\text{mm}\,\text{s}^{-1}$	years	years
Value	10^{-6}	10^{-5}	10^{-3}	10^{-3}	1	0.1	1

$C_R = C_1/2 = \hat{c}$ be addressed in what follows. Under these conditions, it is straightforward to observe that Eqs. (4.23) and (4.25) do not depend on the value of $\hat{c}$ but only on ratios $\hat{c}_a/\hat{c}$ that are herein varied in order to reproduce three modeling scenarios:

Scenario S1 Maintenance of the homeostatic state with $\hat{c}_2 = \hat{c}_3 = \hat{c}$;
Scenario S2 Increased macrophages activity with $\hat{c}_3 = 2\hat{c}$, coupled with a basal production of TGF-β, with $\hat{c}_2 = \hat{c}$;
Scenario S3 Increased macrophages activity with $\hat{c}_3 = 2\hat{c}$ coupled with an increased production of TGF-β from intimal endothelial cells, with $\hat{c}_2 = 1.5\hat{c}$.

For the different scenarios, results are computed via steps 2–4 in Table 4.2 and by employing values of parameters for the transport-remodeling problems summarized in Table 4.4.

4.4.5.1 *Scenario S1*

Concentration profiles $\tilde{c}_q$ obtained from Eqs. (4.23) are shown in Fig. 4.8. Results show that TGF-β (resp., IL) diffuse in aortic thickness starting from the source at the intima-media layer $\rho = 0$ (resp., at the media-adventitial layer $\rho = 1$). The resulting concentrations profiles $\tilde{c}_2$ and $\tilde{c}_3$ respectively represent the consumption and the source terms for MMPs. In turn, the latter exhibit a symmetric concentration profile (due to the symmetry in the employed values of intimal and adventitia permeability $\hat{\lambda}$) with maximum value at $\rho = 0.5$.

Based on the obtained solution for the transport problem, a null remodeling is predicted from Eqs. (4.25) since $\tilde{c}_1(r) \leq C_R$ and $\tilde{c}_2(r) \leq C_R$. Accordingly, since it results $\mathcal{S}(r, t) = \bar{\mathcal{S}}(r)$ for

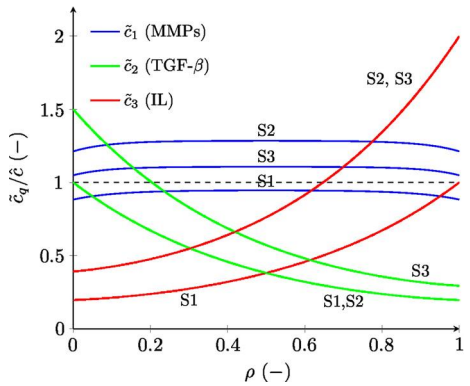

FIGURE 4.8 Normalized concentration profiles $\tilde{c}_q/\hat{c}$ vs. normalized radial coordinate ρ for the scenarios S1, S2 and S3; the dashed line denotes the value $C_{\mathsf{R}}/\hat{c}$ corresponding to the activation of remodeling. Values of parameters in Tables 4.3 and 4.4.

any t, arterial mechanics from Eq. (4.18) results to be constant in time, obtaining the pressure–radius relationship $P_i(r_i, \bar{\mathcal{S}})$, shown in Fig. 4.7, under homeostatic conditions.

4.4.5.2 *Scenario S2*

The increment of macrophages activity is addressed as a possible pathological mechanism and it induces an higher source of IL from the adventitial layer. As shown in Fig. 4.8, a higher concentration of IL is obtained in the media layer from Eqs. (4.23), while TGF-β are clearly unaffected. Accordingly, the source term for MMPs (namely, the average $\tilde{c}_2$ in the overall thickness) increases and $\tilde{c}_1(r) > C_{\mathsf{R}}$ is obtained.

This outcome is associated with remodeling activation in Eqs. (4.25). In particular, the rearrangement of the orientations of collagen fibers (namely, $\beta(r,t)$) is obtained as shown in Fig. 4.6, which corresponds to a more isotropic-distribution of fibers with respect to the homeostatic state. For instance, the number of fibers along the preferred directions $\hat{\beta} = \pm 25°$ decreases up to 40%. Moreover, Fig. 4.9 shows the evolution in time of elastin and collagen volume fraction, as well as of fiber radius, associated with the remodeling. A significant degradation of constituents, whose values nonlinearly evolve in time, is obtained: the greatest degradation is associated with the initial stage of the investigated pathological mechanism and a final decrease of about 30% is obtained in the steady-state at $t = T_{\mathsf{R}}$. In the present scenario, inter-molecular cross-links density is not affected (namely, $\Lambda_c(r,t) = \bar{\Lambda}_c(r)$, corresponding results are not shown for the sake of compactness) because Eq. (4.25d) does not depend on $\tilde{c}_1$ and $\tilde{c}_2(r) \leq C_{\mathsf{R}}$.

As a result of the obtained remodeling, arterial mechanics is significantly affected. The time-dependent pressure–radius relationship $P_i(r_i, \mathcal{S}(r,t))$ along the remodeling path is reported in Fig. 4.9, showing a steady-state enlargement (at $t = T_{\mathsf{R}}$) of about 10% at $P_i = \bar{P}_i$ with respect to $t = 0$.

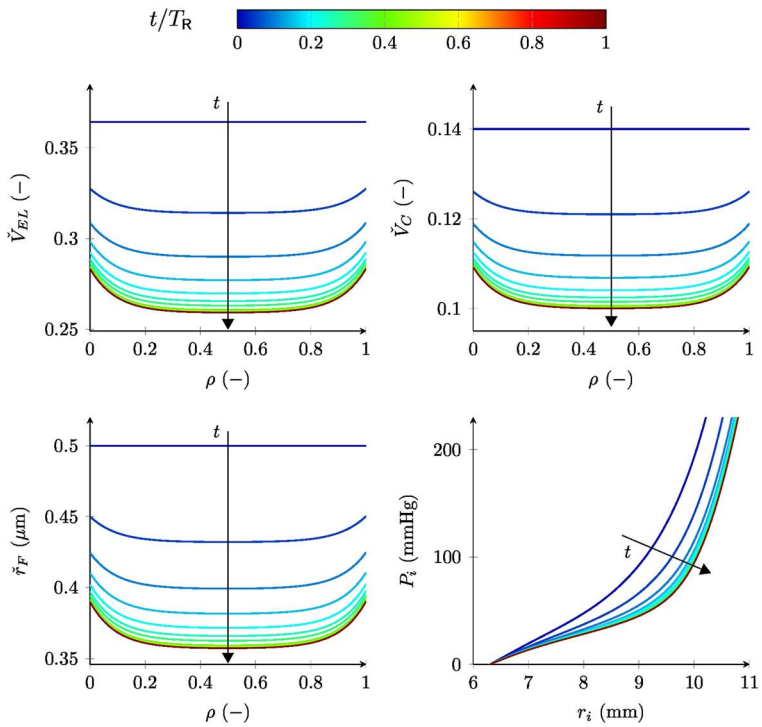

FIGURE 4.9 Scenario S2: time-dependent structural features $s_j(\rho, t)$ and pressure–radius relationship $P_i(r_i, \mathcal{S}(r, t))$ (bottom right); $\check{V}_{EL}$ (top left), average of V_{EL} within media lamellar units (MLUs); $\check{V}_C$ (top right), average of V_C within the interlamellar substance of each MLU; $\check{r}_F$ (bottom left), average of r_F within the interlamellar substance of each MLU. Color map denotes different values of time $t \in [0, T_R]$. Values of parameters in Tables 4.3 and 4.4.

4.4.5.3 *Scenario S3*

The increment in concentrations of both TGF-β and IL with respect to the homeostatic state in scenario S1 (see Fig. 4.8) determines a smaller increase of MMPs concentration with respect to scenario S2.

Nevertheless, since $\tilde{c}_1(r) > C_R$, the degradation of constituents associated with remodeling laws in Eqs. (4.25) is activated. The MMPs-related degradation is anyway mitigated by the depositing properties of TGF-β, since $\tilde{c}_2(r) > C_R$ in about the inner half of arterial thickness. As a matter of fact, the effects of remodeling are shown in Fig. 4.10 where elastin and collagen volume fractions, fiber radius, and inter-molecular cross-links density are shown in the steady-state $t = T_R$, and compared with the ones obtained from different scenarios. Although IL concentration is unaffected with respect to scenario S2, constituents degradation is significantly lower due to the counteracting activity induced by TGF-β. Besides, the value of structural parameters increases in the inner half of arterial thickness, wherein $\tilde{c}_2 > \tilde{c}_1$, and the average variation of the value of structural parameters is less than 10%. In particular, inter-molecular cross-links density increases only because it is not affected by MMPs in the

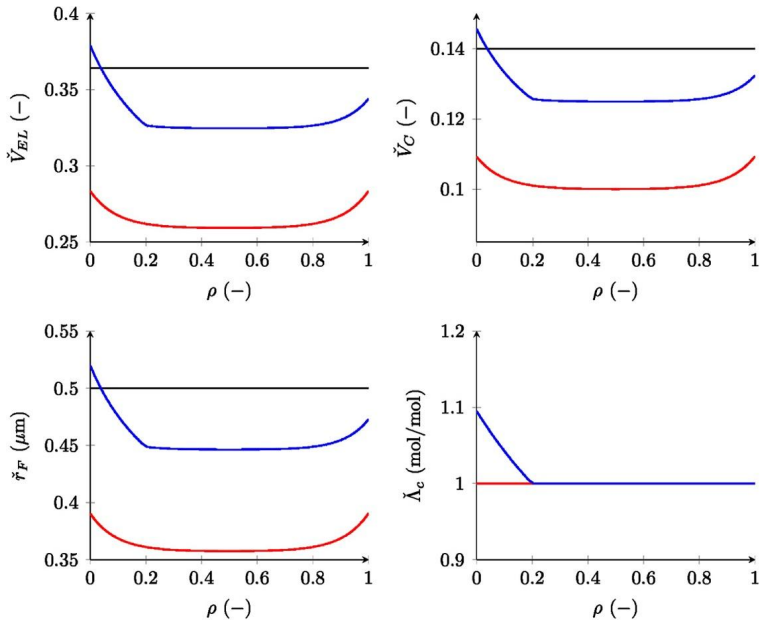

FIGURE 4.10 Structural features $s_j(\rho, T_{\mathsf{R}})$ at steady-state $t = T_{\mathsf{R}}$ for the scenarios S1 (in black), S2 (in red), and S3 (in blue). $\check{V}_{EL}$ (top left), average of V_{EL} within media lamellar units (MLUs); $\check{V}_C$ (top right), average of V_C within the interlamellar substance of each MLU; $\check{r}_F$ (bottom left), average of r_F within the interlamellar substance of each MLU; $\check{\Lambda}_c$ (bottom right), average of Λ_c within the interlamellar substance of each MLU. Values of parameters in Tables 4.3 and 4.4.

present model. Furthermore, as shown in Fig. 4.6, collagen fiber angles are characterized by a symmetric bimodal distribution after the remodeling, similarly to the homeostatic state.

As a consequence, the pressure–radius relationship $P_i(r_i, \mathcal{S}(r, T_{\mathsf{R}}))$ obtained for the present scenario is more similar to the homeostatic scenario S1 than to the pathological one S2 (see Fig. 4.7). In particular, at $P_i = \bar{P}_i$, an aortic enlargement of about 3% is obtained with respect to $t = 0$.

4.5 CONCLUSIONS

Arterial physiopathological behavior involves multiphysics mechanisms, as the result of the complex interplay between microscale transport phenomena and mechanical equilibrium. Indeed, vascular mechanics highly depends on arterial wall constituents whose structural organization and properties are driven by remodeling mechanisms. In turn, the latter are governed by the proteolytic activity of enzymes diffusing within aortic thickness or by cell–cell signaling pathways mediated by soluble factors.

Arterial behavior has been herein modeled and analyzed through a multiphysics strategy that couples macroscopic mechanical description, molecular transport phenomena, and re-

modeling laws of tissue micro- and nano-structural features. Numerical results have been obtained by addressing a case study which shows the effects of ECM remodeling induced by intra-arterial-wall transport of MMPs, TGF-β, and IL on the compliance of an axisymmetric arterial segment.

Remarkably, obtained results show that the present approach is able to capture arterial dilation as a consequence of alterations in tissue biochemical environment and/or cellular activity. For instance, addressing an increased activity of macrophages in the production of cytokines, an enlargement of about 10% is predicted, associated with the proteolytic activity of MMPs. On the other hand, aortic dilation reduce to only 3% when MMPs activity is counterbalanced by TGF-β. This agrees well with available evidence that confirms the protective role of TGF-β whose increased production might represent an internal feedback mechanism or be a consequence of a pharmacological treatment (Dai et al., 2011).

Future studies will address some limitations of present work. The active contraction of smooth muscle cells and the unsteady fluid–structure interaction effects characterizing arterial mechanics have not been considered; no mass growth or constituents turn-over has been investigated; no distinction has been made between latent and active concentrations of molecular species; simplifying assumptions have been introduced (e.g., no mechanical feedback in the transport problem) in order to reduce arterial multiphysics to an open-loop coupled system which can be solved via a staggered and semi-analytical approach.

Acknowledgements

Present research study has been supported by the Italian Minister of University and Research, MIUR (Program: "Consolidate the Foundations 2015"; Project: BIOART; Grant number (CUP): E82F16000850005). Moreover, M. Marino gratefully acknowledges a post-doctoral fellowship from the Alexander von Humboldt Foundation.

APPENDIX A ALONG-THE-CHORD COLLAGEN FIBER TANGENT MODULUS

By following the Maceri–Marino–Vairo multiscale rationale (Maceri et al., 2013; Marino and Vairo, 2013, 2014), the mechanics of crimped collagen fibers is described by introducing an analytical expression for their along-the-chord tangent modulus C_F that depends on main geometric features (period L_F, amplitude H_F, and radius r_F) as well as on material nanoscale mechanisms.

Since fibers are collection of fibrils, material features are described in term of fibril mechanics. Fibril stretch λ_f depends on molecular elongation λ_m (namely, $\lambda_f = \lambda_f(\lambda_m)$) which, in turn, is a function of entropy-related λ_m^s and energy-related λ_m^h molecular stretches (namely, $\lambda_m = \lambda_m(\lambda_m^s, \lambda_m^h)$). Accordingly, fibril elastic modulus E_f results in

$$E_f(\lambda_f) = E_f(\lambda_m^s, \lambda_m^h) = \frac{E_m(\lambda_m^s, \lambda_m^h)\, \Lambda_c\, k_c\, \ell_{m,o}}{[\Lambda_c\, k_c\, \ell_{m,o} + A_m\, E_m(\lambda_m^s, \lambda_m^h)]}\,, \tag{A.1a}$$

with k_c being cross-link stiffness and E_m the elastic modulus of collagen molecules, defined as

$$E_m(\lambda_m) = E_m(\lambda_m^s, \lambda_m^h) = \frac{E_m^s(\lambda_m^s)\, E_m^h(\lambda_m^h)}{E_m^s(\lambda_m^s) + E_m^h(\lambda_m^h)}\,, \tag{A.1b}$$

where entropy-related E_m^s and energy-related E_m^h collagen moduli are

$$E_m^s(\lambda_m^s) = \frac{k_B\, T\, \ell_{m,o}}{\ell_p\, \ell_c\, A_m} \left(\frac{\ell_c^3}{2[\ell_c - \ell_{m,o}\lambda_m^s]^3} + 1 \right), \tag{A.1c}$$

$$E_m^h(\lambda_m^h) = \frac{\ell_{m,o}}{\ell_c} \left[\frac{\hat{E}}{1 + \exp\{-\eta[\ell_{m,o}(\lambda_m^h - 1)/\ell_c - \varepsilon_o^h]\}} + \hat{E}_o \right], \tag{A.1d}$$

with k_B being the Boltzmann constant and T the absolute temperature. Other symbols are defined in Section 4.3.3.1. The multiscale problem is closed via interscale compatibility relationships between atomistic- and nanoscales:

$$\frac{d\lambda_m^s}{d\lambda_m} = \Phi_{ms}(\lambda_m^s, \lambda_m^h) = \frac{E_m(\lambda_m^s, \lambda_m^h)}{E_m^s(\lambda_m^s)}\,, \tag{A.2a}$$

$$\frac{d\lambda_m^h}{d\lambda_m} = \Phi_{mh}(\lambda_m^s, \lambda_m^h) = \frac{E_m(\lambda_m^s, \lambda_m^h)}{E_m^h(\lambda_m^h)}\,, \tag{A.2b}$$

and between nanoscale and mesoscale:

$$\frac{d\lambda_m}{d\lambda_f} = \Phi_{fm}(\lambda_m^s, \lambda_m^h) = \frac{E_f(\lambda_m^s, \lambda_m^h)}{E_m(\lambda_m^s, \lambda_m^h)}\,. \tag{A.3}$$

A closed-form expression for C_F can be obtained from the application of the Principle of Virtual Works by assuming a piecewise-linear fiber-shape and by coupling geometric and material nonlinearities (Marino and Wriggers, 2016). Geometric nonlinearities are introduced by accounting for the functional dependence of fiber amplitude on along-the-chord fiber elongation λ_F, namely $H_F = H_F(\lambda_F)$. Moreover, by definition, it results in $L_F = L_F(\lambda_F) = \lambda_F L_{F,o}$ where $L_{F,o}$ represents fiber period in the reference configuration. Material nonlinearities are accounted for by means of fibril tangent modulus $E_f = E_f(\lambda_f) = E_f(\lambda_m^s, \lambda_m^h)$ in Eqs. (A.1). In order to couple material nonlinearities with geometric ones, an inter-scale compatibility relationship between fibril stretch λ_f and along-the-chord fiber stretch λ_F is introduced by identifying λ_f as coincident with the stretch of the fiber centerline, resulting in

$$\frac{d\lambda_f}{d\lambda_F} = \Phi_f(\lambda_F, H_F) = \frac{\lambda_F \ell_{F,o}^2 + H_F \frac{dH_F}{d\lambda_F}}{\sqrt{(\lambda_F^2 \ell_{F,o}^2 + H_F^2)(\ell_{F,o}^2 + H_{F,o}^2)}}, \tag{A.4}$$

where $\ell_F = L_F/4$ is the fiber quarter-period and $H_{F,o}$ is the fiber amplitude in the reference configuration.

Therefore, omitting functional dependencies for the sake of compactness, it results in

$$C_F = E_f \frac{\ell_F^2 + H_F^2}{\sqrt{\ell_{F,o}^2 + H_{F,o}^2}} \left[\ell_F + \frac{4H_F^2}{3r_F^2 \ell_F} \left(\ell_F^2 + H_F^2 \right) \right]^{-1}, \tag{A.5}$$

coupled with the following interscale differential equations:

$$\frac{d\lambda_m^s}{d\lambda_F} = \Phi_{ms}(\lambda_m^s, \lambda_m^h)\Phi_{fm}(\lambda_m^s, \lambda_m^h)\Phi_f(\lambda_F, H_F), \tag{A.6a}$$

$$\frac{d\lambda_m^h}{d\lambda_F} = \Phi_{mh}(\lambda_m^s, \lambda_m^h)\Phi_{fm}(\lambda_m^s, \lambda_m^h)\Phi_f(\lambda_F, H_F), \tag{A.6b}$$

$$\frac{dH_F}{d\lambda_F} = -\frac{\ell_F H_F \left[4(\ell_F^2 + H_F^2) - 3r_F^2\right]}{\lambda_F \left[4H_F^2(\ell_F^2 + H_F^2) + 3\ell_F^2 r_F^2\right]}, \tag{A.6c}$$

where Eqs. (A.2), (A.3), and (A.4) are taken into account. Accordingly, from the solution of the system of differential equations (A.6), functions $\lambda_m^s = \lambda_m^s(\lambda_F)$, $\lambda_m^h = \lambda_m^h(\lambda_F)$, and $H_F = H_F(\lambda_F)$ are obtained, resulting in $C_F = C_F(\lambda_F)$. Moreover, in order to highlight the explicit dependence of predicted fiber mechanics on the set of structural parameters $\mathcal{S}_F$ (defined in Eqs. (4.4)), the functional form $C_F = C_F(\lambda_F, \mathcal{S}_F)$ is conveniently employed.

APPENDIX B MICROSTRUCTURE OF AORTIC MEDIA LAYER

Aortic media layer is modeled as comprising N_M iso-width perfectly-bonded layers representing a single media lamellar unit (MLU). Each of them comprises n_M iso-width perfectly-bonded sub-layers. Accordingly, $s_j \in \mathcal{S}$ are piecewise constant functions in r where, for the sake of notation, $s_j^{k,p}$ denotes the value of s_j in the pth sub-lamella of the kth lamella. Moreover, let subscript k take values in $\{1, \ldots, N_M\}$, p in $\{1, \ldots, n_M\}$, and c in $\{2, \ldots, n_M\}$.

The kth lamella is considered as made up of one elastin layer (namely, $V_C^{k,1} = 0$) and $n_M - 1$ sub-lamellae reinforced by collagen fibers ($V_C^{k,c} > 0$).

For describing the homeostatic state, let us introduce $\bar{V}_{EL}^{el}$, $\bar{V}_{EL}^{is}$, and $\bar{V}_C^{is}$ as constant values. The elastin layer is assumed to be characterized by $\bar{V}_{EL}^{k,1} = \bar{V}_{EL}^{el}$ for any MLU (namely, for any $k = 1, \ldots, N_M$). Moreover, we choose $\bar{V}_{EL}^{k,p} = \bar{V}_{EL}^{is}$ and $\bar{V}_C^{k,c} = \bar{V}_C^{is}$, constant within and among MLUs. Furthermore, the homeostatic orientation of collagen fibers in the inter-lamellar substance at the reference configuration is defined by the function $\bar{\beta}_o = \bar{\beta}_o(r)$, with

$$\bar{\beta}_o^{k,c} = \varpi_k(r)\vartheta_{c-1}^{ani}(\hat{\beta}) + (1 - \varpi_k(r))\vartheta_{c-1}^{iso} \tag{B.1a}$$

where

$$\varpi_k(r) = \begin{cases} 2(\rho_k(r) - r_i)/(r_e - r_i) & \text{for } \rho_k(r) < (r_e + r_i)/2, \\ 1 & \text{for } \rho_k(r) \geq (r_e + r_i)/2, \end{cases} \tag{B.1b}$$

$$\rho_k(r) = (r_{e,k} + r_{i,k})/2 \quad \text{for } r_{i,k} \leq r < r_{e,k}\,, \tag{B.1c}$$

$$r_{i,k} = r_i + (k-1)(r_e - r_i)/N_M\,, \tag{B.1d}$$

$$r_{e,k} = r_{i,k} + (r_e - r_i)/N_M\,, \tag{B.1e}$$

and ϑ^{ani}_{c-1} (resp., ϑ^{iso}_{c-1}) is the $(c-1)$th component of vector $\boldsymbol{\vartheta}^{ani}(\hat{\beta}) \in \mathbb{R}^{n_M-1}$ (resp., $\boldsymbol{\vartheta}^{iso} \in \mathbb{R}^{n_M-1}$) representing a fiber angle distribution with preferred direction $\hat{\beta} \in (0, \pi/2)$ (resp., without any preferred direction). In the numerical simulations conducted in the present work, we choose $n_M = 18$ and

$$\boldsymbol{\vartheta}^{iso} = (-\hat{\boldsymbol{\vartheta}}^{iso}, 0, \hat{\boldsymbol{\vartheta}}^{iso})\,, \qquad \boldsymbol{\vartheta}^{ani}(\bar{\beta}^*) = (-\hat{\boldsymbol{\vartheta}}^{ani}(\hat{\beta}), 0, \hat{\boldsymbol{\vartheta}}^{ani}(\hat{\beta}))\,, \tag{B.1f}$$

where

$$\hat{\boldsymbol{\vartheta}}^{iso} = (10, 20, 30, 40, 50, 60, 70, 80)\pi/180\,, \tag{B.1g}$$

$$\hat{\boldsymbol{\vartheta}}^{ani}(\hat{\beta}) = (1/2, 2/3, 2/3, 1, 1, 1, 4/3, 5/3)\,\pi\hat{\beta}/180\,. \tag{B.1h}$$

Finally, for the sake of describing the remodeling of fiber orientation, let β_{iso} in Eq. (4.24e) be a piecewise constant function with values

$$\beta^{k,c}_{iso} = \vartheta^{iso}_{c-1}\,. \tag{B.2}$$

References

Auricchio, F., Da Veiga, L.B., Lovadina, C., Reali, A., Taylor, R.L., Wriggers, P., 2013. Approximation of incompressible large deformation elastic problems: some unresolved issues. Comput. Mech. 52 (5), 1153–1167.

Auricchio, F., Conti, M., Ferrara, A., 2014. How constitutive model complexity can affect the capability to fit experimental data: a focus on human carotid arteries and extension/inflation data. Arch. Comput. Methods Eng. 21 (3), 273–292.

Baek, S., Rajagopal, K.R., Humphrey, J.D., 2006. A theoretical model of enlarging intracranial fusiform aneurysms. J. Biomech. Eng. 128 (1), 142–149.

Bailey, A.J., 2001. Molecular mechanisms of ageing in connective tissues. Mech. Ageing Dev. 122 (7), 735–755.

Behmoaras, J., Osborne-Pellegrin, M., Gauguier, D., Jacob, M.P., 2005. Characteristics of the aortic elastic network and related phenotypes in seven inbred rat strains. Am. J. Physiol., Heart Circ. Physiol. 288 (2), H769–H777.

Brüel, A., Ørtoft, G., Oxlund, H., 1998. Inhibition of cross-links in collagen is associated with reduced stiffness of the aorta in young rats. Atherosclerosis 140 (1), 135–145.

Buehler, M.J., Wong, S.Y., 2007. Entropic elasticity controls nanomechanics of single tropocollagen molecules. Biophys. J. 93 (1), 37–43.

Carmo, M., Colombo, L., Bruno, A., Corsi, F.R.M., Roncoroni, L., Cuttin, M.S., Radice, F., Mussini, E., Settembrini, P.G., 2002. Alteration of elastin, collagen and their cross-links in abdominal aortic aneurysms. Eur. J. Vasc. Endovasc. Surg. 23 (6), 543–549.

Clark, J.M., Glagov, S., 1985. Transmural organization of the arterial media. The lamellar unit revisited. Arterioscler. Thromb. Vasc. Biol. 5 (1), 19–34.

Chen, H., Liu, Y., Slipchenko, M.N., Zhao, X., Cheng, J.X., Kassab, G.S., 2011. The layered structure of coronary adventitia under mechanical load. Biophys. J. 101 (11), 2555–2562.

Dabagh, M., Jalali, P., Tarbell, J.M., 2009. The transport of LDL across the deformable arterial wall: the effect of endothelial cell turnover and intimal deformation under hypertension. Am. J. Physiol., Heart Circ. Physiol. 297, H983–H996.

Dai, J., Michineau, S., Franck, G., Desgranges, P., Becquemin, J.P., Gervais, M., Allaire, E., 2011. Long term stabilization of expanding aortic aneurysms by a short course of cyclosporine a through transforming growth factor-beta induction. PLoS ONE 6, e28903.

Deguchi, J.O., Aikawa, E., Libby, P., Vachon, J.R., Inada, M., Krane, S.M., Whittaker, P., Aikawa, M., 2005. Matrix metalloproteinase-13/collagenase-3 deletion promotes collagen accumulation and organization in mouse atherosclerotic plaques. Circulation 112, 2708–2715.

D'Errico, M., Sammarco, P., Vairo, G., 2015. Analytical modeling of drug dynamics induced by eluting stents in the coronary multi-layered curved domain. Math. Biosci. 267, 79–96.

Ethier, C.R., Simmons, C.A., 2007. Introductory Biomechanics – From Cells to Organisms. Cambridge University Press, Cambridge.

Farlow, S.J., 1982. Partial Differential Equations for Scientists and Engineers. Wiley, New York.

Figueroa, C.A., Baek, S., Taylor, C.A., Humphrey, J.D., 2009. A computational framework for coupled fluid–solid growth modeling in cardiovascular simulations. Comput. Methods Appl. Mech. Eng. 198 (45), 3583–3602.

Fratzl, P., 2008. Collagen: Structure and Mechanics. Springer, New York.

Freedman, B.R., Bade, N.D., Riggin, C.N., Zhang, S., Haines, P.G., Ong, K.L., Janmey, P.A., 2015. The (dys)functional extracellular matrix. Biochim. Biophys. Acta, Mol. Cell Res. 1853 (11), 3153–3164.

Fuster, V., Kelly, B., 2010. Promoting Cardiovascular Health in the Developing World: A Critical Challenge to Achieve Global Health. National Academies Press, Washington DC.

García-Alvarez, J., Ramirez, R., Checa, M., Nuttall, R.K., Sampieri, C.L., Edwards, D.R., Selman, M., Pardo, A., 2006. Tissue inhibitor of metalloproteinase-3 is up-regulated by transforming growth factor-β1 in vitro and expressed in fibroblastic foci in vivo in idiopathic pulmonary fibrosis. Exp. Lung Res. 32, 201–214.

Hallock, P., Benson, I.C., 1937. Studies on the elastic properties of human isolated aorta. J. Clin. Invest. 16 (4), 595–602.

Holzapfel, G.A., Ogden, R.W., 2010. Modelling the layer-specific three-dimensional residual stresses in arteries, with an application to the human aorta. J. R. Soc. Interface 7, 787–799.

Holzapfel, G.A., Gasser, T.C., Ogden, R.W., 2000. A new constitutive framework for arterial wall mechanics and a comparative study of material models. J. Elast. 61 (1–3), 1–48.

Humphrey, J.D., 2002. Cardiovascular Solid Mechanics: Cells, Tissues, and Organs. Springer, New York.

Humphrey, J.D., Rajagopal, K.R., 2002. A constrained mixture model for growth and remodeling of soft tissues. Math. Models Methods Appl. Sci. 12 (3), 407–430.

Humphrey, J.D., 2009. Vascular mechanics, mechanobiology, and remodeling. J. Mech. Med. Biol. 9 (2), 243–257.

Jones, J.A., Spinale, F.G., Ikonomidis, J.S., 2009. Transforming growth factor-β signaling in thoracic aortic aneurysm development: a paradox in pathogenesis. J. Vasc. Res. 46 (2), 119–137.

Kassab, G.S., 2006. Biomechanics of the cardiovascular system: the aorta as an illustratory example. J. R. Soc. Interface 3, 719–740.

Kucich, U., Rosenbloom, J.C., Abrams, W.R., Rosenbloom, J., 2002. Transforming growth factor-β stabilizes elastin mRNA by a pathway requiring active Smads, protein kinase C-δ, and p38. Am. J. Respir. Cell Mol. Biol. 26 (2), 183–188.

Lee, E., Grodzinsky, A.J., Libby, P., Clinton, S.K., Lark, M.W., Lee, R.T., 1995. Human vascular smooth muscle cell–monocyte interactions and metalloproteinase secretion in culture. Arterioscler. Thromb. Vasc. Biol. 15 (12), 2284–2289.

Leemasawatdigul, K., Gappa-Fahlenkamp, H., 2012. Development of a mathematical model to describe the transport of monocyte chemoattractant protein-1 through a three-dimensional collagen matrix. Cardiovasc. Pathol. 21 (3), 219–228.

Lilly, B., 2014. We have contact: endothelial cell–smooth muscle cell interactions. Physiology 29 (4), 234–241.

Maceri, F., Marino, M., Vairo, G., 2012. Elasto-damage modeling of biopolymer molecules response. Comput. Model. Eng. Sci. 87, 461–481.

Maceri, F., Marino, M., Vairo, G., 2013. Age-dependent arterial mechanics via a multiscale elastic approach. Int. J. Comput. Methods Eng. Sci. Mech. 14, 141–151.
Maiellaro, K., Taylor, W.R., 2007. The role of the adventitia in vascular inflammation. Cardiovasc. Res. 75 (4), 640–648.
Marino, M., Vairo, G., 2013. Multiscale elastic models of collagen bio-structures: from cross-linked molecules to soft tissues. In: Gefen, A. (Ed.), Multiscale Computer Modeling in Biomechanics and Biomedical Engineering. Springer, Berlin, Heidelberg.
Marino, M., Vairo, G., 2014. Computational modelling of soft tissues and ligaments. In: Jin, Z. (Ed.), Computational Modelling of Biomechanics and Biotribology in the Musculoskeletal System. Woodhead Publishing, Cambridge.
Marino, M., 2016. Molecular and intermolecular effects in collagen fibril mechanics: a multiscale analytical model compared with atomistic and experimental studies. Biomech. Model. Mechanobiol. 15, 133–154.
Marino, M., Wriggers, P., 2016. Finite strain response of crimped beams under uniaxial traction: an analytical approach applied to collagen. J. Mech. Phys. Solids. http://dx.doi.org/10.1016/j.jmps.2016.05.010. In press.
Merrilees, M.J., Tiang, K.M., Scott, 1987. Changes in collagen fibril diameters across artery walls including a correlation with glycosaminoglycan content. Connect. Tissue Res. 16 (3), 237–257.
Michel, J.B., Thaunat, O., Houard, X., Meilhac, O., Caligiuri, G., Nicoletti, A., 2007. Topological determinants and consequences of adventitial responses to arterial wall injury. Arterioscler. Thromb. Vasc. Biol. 27 (6), 1259–1268.
Nardinocchi, P., Teresi, L., 2007. On the active response of soft living tissues. J. Elast. 88 (1), 27–39.
O'Connell, M.K., Murthy, S., Phan, S., Xu, C., Buchanan, J., Spilker, R., Dalman, R.L., Zarins, C.K., Denk, W., Taylor, C.A., 2008. The three-dimensional micro- and nanostructure of the aortic medial lamellar unit measured using 3D confocal and electron microscopy imaging. Matrix Biology 27, 171–181.
Pontrelli, G., De Monte, F., 2007. Mass diffusion through two-layer porous media: an application to the drug-eluting stent. Int. J. Heat Mass Transf. 50 (17), 3658–3669.
Rachev, A., Stergiopulos, N., Meister, J.J., 1996. Theoretical study of dynamics of arterial wall remodeling in response to changes in blood pressure. J. Biomech. 29, 635–642.
Rastogi, A., Kim, H., Twomey, J.D., Hsieh, A.H., 2013. MMP-2 mediates local degradation and remodeling of collagen by annulus fibrosus cells of the intervertebral disc. Arthritis Res. Ther. 15 (2), 1.
Rezakhaniha, R., Fonck, E., Genoud, C., Stergiopulos, N., 2011. Role of elastin anisotropy in structural strain energy functions of arterial tissue. Biomech. Model. Mechanobiol. 10 (4), 599–611.
Sagi, I., Gaffney, J.P. (Eds.), 2015. Matrix Metalloproteinase Biology. Wiley, Hoboken.
Sasaki, N., Odajima, S., 1996. Elongation mechanism of collagen fibrils and force–strain relations of tendon at each level of structural hierarchy. J. Biomech. 29, 1131–1136.
Schriefl, A.J., Zeindlinger, G., Pierce, D.M., Regitnig, P., Holzapfel, G.A., 2012. Determination of the layer-specific distributed collagen fibre orientations in human thoracic and abdominal aortas and common iliac arteries. J. R. Soc. Interface 9, 1275–1286.
Svensson, R.B., Mulder, H., Kovanen, V., Magnusson, S.P., 2013. Fracture mechanics of collagen fibrils: influence of natural cross-links. Biophys. J. 104, 2476–2484.
Tarbell, J.M., 2003. Mass transport in arteries and the localization of atherosclerosis. Annu. Rev. Biomed. Eng. 5 (1), 79–118.
Taylor, C.A., Humphrey, J.D., 2009. Open problems in computational vascular biomechanics: hemodynamics and arterial wall mechanics. Comput. Methods Appl. Mech. Eng. 198, 3514–3523.
Truskey, G.A., Yuan, F., Katz, D.F., 2010. Transport Phenomena in Biological Systems. Pearson Prentice Hall Bioengineering. Pearson Education, New Jersey, USA.
Vairo, G., Cioffi, M., Cottone, R., Dubini, G., Migliavacca, F., 2010. Drug release from coronary eluting stents: a multidomain approach. J. Biomech. 43, 1580–1589.
Vandermeer, J., 2010. How populations grow: the exponential and logistic equations. Nat. Educ. Knowl. 3 (10), 15.
van der Slot, A.J., Van Dura, E.A., De Wit, E.C., Degroot, J., Huizinga, T.W.J., Bank, R.A., Zuurmond, A.M., 2005. Elevated formation of pyridinoline cross-links by profibrotic cytokines is associated with enhanced lysyl hydroxylase 2b levels. Biochim. Biophys. Acta, Mol. Basis Dis. 1741 (1), 95–102.
Visse, R., Nagase, H., 2003. Matrix metalloproteinases and tissue inhibitors of metalloproteinases structure, function, and biochemistry. Circ. Res. 92 (8), 827–839.
Volokh, K.Y., Vorp, D.A., 2008. A model of growth and rupture of abdominal aortic aneurysm. J. Biomech. 41 (5), 1015–1021.
Wada, S., Karino, T., 1999. Theoretical study on flow-dependent concentration polarization of low density lipoproteins at the luminal surface of a straight artery. Biorheology 36, 207–233.

Watton, P.N., Ventikos, Y., Holzapfel, G.A., 2009. Modelling the growth and stabilization of cerebral aneurysms. Math. Med. Biol. 26 (2), 133–164.
Wolinsky, H., Glagov, S., 1964. Structural basis for the static mechanical properties of the aortic media. Circ. Res. 14 (5), 400–413.
Wolinsky, H., Glagov, S., 1967. A lamellar unit of aortic medial structure and function in mammals. Circ. Res. 20 (1), 99–111.
Wriggers, P., 2008. Nonlinear Finite Element Methods. Springer, Berlin, Heidelberg.
Zhang, W., Herrera, C., Atluri, S.N., Kassab, G.S., 2005. The effect of longitudinal pre-stretch and radial constraint on the stress distribution in the vessel wall: a new hypothesis. Mech. Chem. Biosyst. 2, 41–52.